Paleomagnetism of the Datong monogenetic volcanoes in China: paleodirection and paleointensity during the middle to early Brunhes Chron

Y. Yamamoto[1]*, H. Tsunakawa[2], J. Shaw[1], and M. Kono[2]

[1]*Geomagnetism Laboratory, Department of Earth and Ocean Sciences, University of Liverpool, L69 7ZE, United Kingdom*
[2]*Department of Earth and Planetary Sciences, Tokyo Institute of Technology, Tokyo 152-8551, Japan*

Paleomagnetic measurements were conducted on Datong volcanic rocks from China, which are thought to have formed in the mid to early Brunhes Chron. Meaningful site-mean paleodirections were obtained from 21 sites which are considered to represent 17 independent cooling units. They give a mean VGP (virtual geomagnetic pole) position of (76.5°N, 7.9°E) with A_{95}=7.7° (N=17), which is statistically distinct from geographic north. This dataset also yields an ASD (angular standard deviation) of 17.2° around the mean VGP position. Because the paleodirections form two clusters, the samples may record the paleomagnetic field during two different short periods and therefore may not average out paleosecular variation. Paleointensity measurements were conducted using three different methods. The DHT and LTD-DHT Shaw methods, the Thellier method, and the microwave Thellier method were applied to 119, 29 and 73 specimens respectively, and they give 66, 16 and 12 successful results (success rates are 55, 55 and 16%). From the LTD-DHT Shaw dataset, eight acceptable site-mean paleointensities are obtained. They give an average VDM (virtual dipole moment) of $3.79 \pm 1.94 \times 10^{22}$ A m^2. This is 56% lower than the average VDM of $5.91 \pm 1.74 \times 10^{22}$ A m^2 (N=14) calculated from the selected Thellier data from the latest paleointensity database using the same criteria. One possible reason for this difference might be systematic overestimations of paleointensities by the Thellier method on volcanic rocks.
Key words: Paleosecular variation, paleointensity, LTD-DHT Shaw method, Datong Volcano, Brunhes Chron.

1. Introduction

The magnetic field generated by the geodynamo is one of the most important features of the Earth. The geomagnetic field can be approximated by a time varying dipole field and it is important to know how the geomagnetic dipole moment has varied in the past by measuring absolute paleointensities (ancient geomagnetic field strengths) from volcanic rocks. Since the 1970s, the Thellier-Thellier (Thellier and Thellier, 1959) and the Shaw (Shaw, 1974) types of paleointensity methods have been most commonly used. After the 1990s, however, most paleomagnetists have regarded the Thellier-type method as the most reliable (e.g. Selkin and Tauxe, 2000; Goguitchaichvili *et al.*, 2004). Recent discussions on past geomagnetic dipole moments (e.g. Goguitchaichvili *et al.*, 2004) are mostly based on the global paleointensity dataset obtained by the Thellier method with pTRM checks (Thellier and Thellier 1959; Coe *et al.*, 1978). If only the Thellier results are considered from the latest paleointensity database (Perrin and Schnepp, 2004), the time-averaged geomagnetic dipole moment is estimated to be 7.46×10^{22} A m^2 for the last 5 million years (Yamamoto and Tsunakawa, 2005). It is almost the same value as the present geomagnetic dipole moment ($\sim 8 \times 10^{22}$ A m^2), indicating that characteristics of the present-day field are typical of the geomagnetic field during this geologically recent period.

However, recent studies have revealed that natural rock samples may not always be the ideal material for the Thellier method: evidence is accumulating which indicates that the Thellier method is not always suitable for historical lava flows, resulting in systematically high paleointensities (Hill and Shaw, 2000; Calvo *et al.*, 2002; Yamamoto *et al.*, 2003; Mochizuki *et al.*, 2004; Oishi *et al.*, 2005). Alternatively, Tsunakawa and Shaw (1994) and Yamamoto *et al.* (2003) have developed a significantly improved version of the original Shaw method (Shaw, 1974), i.e. the LTD-DHT Shaw method. This method has been successfully applied to several historical lava flows (Yamamoto *et al.*, 2003; Mochizuki *et al.*, 2004; Oishi *et al.*, 2005).

Yamamoto and Tsunakawa (2005) obtained controversial paleointensity results from volcanic rocks from the Society Islands, French Polynesia (southern hemisphere). The LTD-DHT Shaw method gave an average geomagnetic dipole moment of 3.64×10^{22} A m^2 for the last 5 million years. This is nearly half of the previous estimate based on the reported Thellier data and also half the present dipole moment. This result suggests that the present-day field is so strong that it may not be typical of the paleomagnetic field.

Because the geomagnetic field is a global phenomenon, it is expected that similar paleointensities would be observed from volcanic rocks of the northern hemisphere. One approach to obtain new paleointensities from the last 5 mil-

*Now at Center for Advanced Marine Core Research, Kochi University, Kochi 783-8502, Japan.
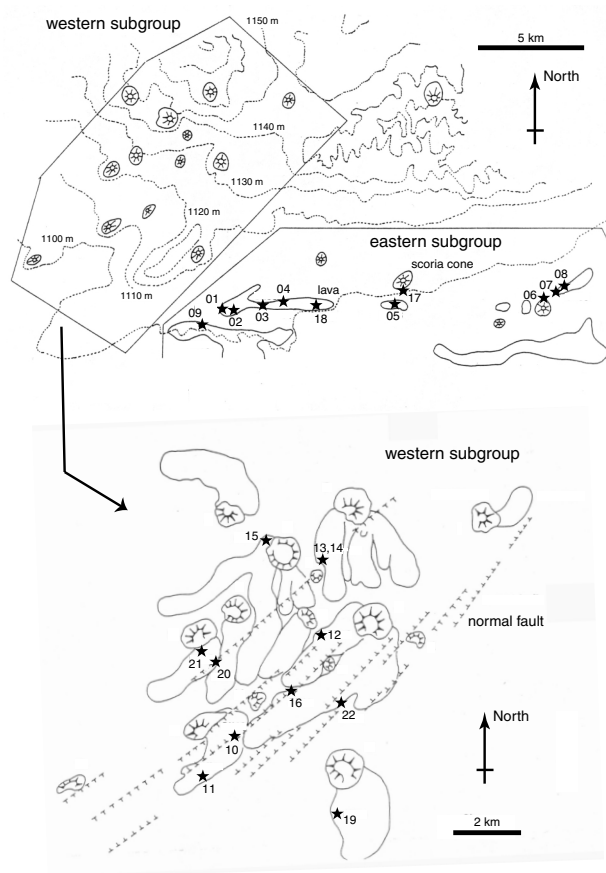
Fig. 1. Map showing the sampling sites. Palaeomagnetic core samples were collected at 22 sites of the eastern and the western subgroups. Numbers indicate the site IDs (DX01–DX22).

Fig. 2. Four types of thermomagnetic curves. Solid and dotted curves indicate heating and cooling curves, respectively.

lion years is to conduct the LTD-DHT Shaw experiments on samples from various volcanoes located in the northern hemisphere. In this paper, we report new LTD-DHT Shaw paleointensities from the Datong volcanoes in China of middle to early Brunhes age. In order to cross-check the results, we also perform paleointensity measurements using the conventional Thellier method as well as the microwave Thellier method.

2. Geology and Sampling Sites

The Datong monogenetic volcanoes are located within the Datong Basin in the Shanxi Rift Zone (40.0–40.1°N and 113.6–113.9°E). The basin and its marginal upland areas are composed of rocks with various geological ages from Archean to Holocene. The rifting of the Datong Basin began during the Miocene and has continued to the present day (Bureau of Geology and Mineral Resources of Shanxi Province, 1989; Cheng *et al.*, 2006). Several studies of fault tectonic geomorphology and paleoseismology indicate intense Holocene activity of the basin-bounding faults (Deng *et al.*, 1994; Duan and Fang, 1995; Xu *et al.*, 1996; Cheng and Yang, 1999; Cheng *et al.*, 2006). Within the field area there were two recent large earthquakes, one on October 18 in 1989 (magnitude 6.5) and one on March 26 in 1991 (magnitude 5.8) (Cheng *et al.*, 2006).

The Datong volcanoes consist of more than 30 volcanic cones within an area of about 50 km^2. They are composed
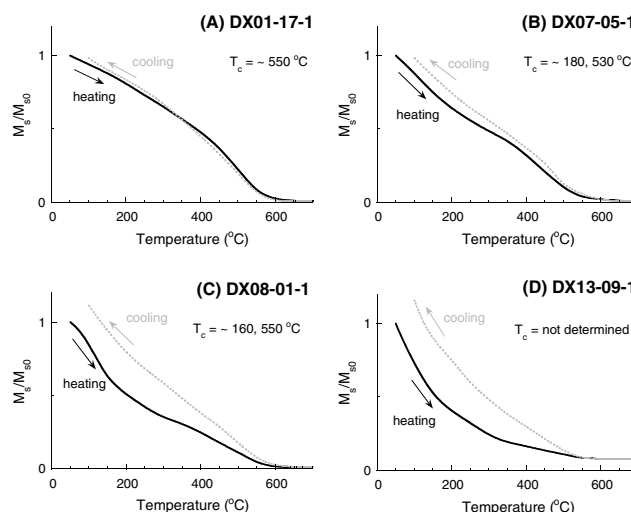
of alkaline basalts erupted from volcanic cones, tholeiites erupted along buried basement faults, and other pyroclastics (Chen *et al.*, 1992; Liu *et al.*, 2002; Cheng *et al.*, 2006). Hurford and Chen (1986) reported that 21 whole-rock basalt samples collected from the Datong volcanoes give K-Ar ages ranging between 0.227 and 0.822 Ma and that the major period of volcanism is 0.3–0.4 Ma. These ages are consistent with those obtained in later studies: 0.74±0.22 Ma, 0.60±0.15 Ma, 0.54±0.05 Ma, 0.41±0.10 Ma, and 0.25±0.04 Ma (Kaneoka *et al.*, 1983; Chen *et al.*, 1992; Cheng *et al.*, 2006). There are two groups of volcanoes: one is distributed along a NE-SW trend (western subgroup) while the other aligns along an EW direction (eastern subgroup) (Fig. 1). In the area of the western subgroup, normal faults develop along the NE-SW trend. Formation ages of the faults are considered to be older than the volcanic eruptions because grabens formed by the faults are buried with lavas. The active age of the eastern subgroup is thought to be older than that of the western subgroup since the degree of erosion in volcanic cones is high in the eastern subgroup.

Paleomagnetic core samples were collected at 22 sites of alkaline basalt in October 1987 (DX01–DX22; Fig. 1). Sample collection was done using a portable gasoline-powered drill and the core orientation was made by both sun and magnetic compasses. Because vegetations sometimes developed between outcrops of the sampling sites, some of the sites possibly belong to the same cooling unit: for instance, the sites DX01, 02, 03, 04 and 18 in the eastern subgroup. They are tentatively classified as the same lava flow in Fig. 1.

3. Rock Magnetic Property

Thermomagnetic analyses were carried out on one sample per flow (total 22 samples) in air using a Curie balance. The resultant Ms-T curves could be classified into four types: A, B, C and D (Fig. 2 and Table 1). They indicate that the main magnetic carrier is titanomagnetite with different Ti contents. Type A curves were observed

Table 1. Statistical results of the paleodirections and the LTD-DHT Shaw dataset.

Site	Ms-T type	N_d	Dec (°)	Inc (°)	α_{95} (°)	P_{Lat} (°)	P_{Long} (°)	N_F	F (μT)	VDM (10^{22} A m²)	VADM (10^{22} A m²)	ΔAIC_{min}
eastern subgroup (40.0°N, 113.7–113.9°E)												
DX01	A	15	315.5	57.1	3.0	55.6	34.5	5	15.6±3.5	2.77±0.62	2.70±0.60	−2.0
DX03	A	12	311.5	58.8	3.3	53.2	39.0	3	12.4±2.8	2.15±0.48	2.14±0.48	−1.3
DX01+03		*27*	*313.8*	*57.9*	*2.2*	*54.6*	*36.5*	*8*	*14.4±3.5*	*2.53±0.61*	*2.49±0.60*	
DX04m	A	13	323.0	62.2	2.3	62.4	43.2	4	16.9±2.0	2.82±0.34	2.93±0.35	−1.0
DX18	A	8	324.5	63.7	3.3	63.6	47.2	3	19.1±2.9	3.12±0.47	3.31±0.50	8.1
DX04+18		*21*	*323.5*	*62.8*	*1.8*	*62.9*	*44.7*	*7*	*17.8±2.5*	*2.95±0.41*	*3.09±0.43*	
DX02	A	13	333.2	62.5	2.3	69.8	43.6	5	6.80±1.52	1.13±0.25	1.18±0.26	−2.0
DX05	C	14	352.0	41.5	2.2	72.5	318.6	2	11.2	2.37	1.93	−1.9
DX06	A	14	356.8	52.5	5.1	82.6	315.1	7	23.2±7.3	4.37±1.38	4.02±1.27	−2.0
DX07	B	11	351.9	44.5	2.3	74.6	322.3	7	13.6±1.6	2.80±0.33	2.36±0.28	−1.9
DX08	C	8	348.9	35.8	2.8	67.7	322.3	5	17.9±2.0	3.99±0.46	3.10±0.35	−1.8
DX09	B	7	334.8	68.7	3.4	68.9	67.1	4	18.3±1.0	2.80±0.16	3.17±0.18	6.9
DX17	C	7	351.1	24.0	5.8	61.4	312.2	3	14.6±2.3	3.54±0.55	2.53±0.39	1.7
western subgroup (40.0–40.1°N, 113.6–113.7°E)												
DX13	D	8	352.5	40.6	2.5	72.0	316.4	4	52.4±10.7	11.2±2.30	9.08±1.86	−2.0
DX14	C	7	356.8	45.1	9.5	76.3	305.6	1	26.6	5.44	4.60	13.3
DX13+14		*15*	*354.4*	*42.7*	*4.3*	*74.0*	*312.2*	*5*	*47.3±14.9*	*9.92±3.12*	*8.18±2.57*	
DX16	A	9	312.7	68.2	4.9	55.8	59.0	1	53.0	8.18	9.18	21.1
DX22	C	9	324.4	68.4	5.4	63.0	61.1	2	45.1	6.93	7.81	32.5
DX16+22		*18*	*318.5*	*68.4*	*3.5*	*59.4*	*59.9*	*3*	*47.7±4.6*	*7.34±0.70*	*8.27±0.79*	
DX10	A	9	347.1	52.1	4.0	77.3	352.2	5	27.3±6.8	5.18±1.29	4.73±1.18	−1.9
DX11	D	8	327.0	54.0	5.9	63.3	382.2	3	31.2±5.2	5.78±0.95	5.41±0.89	−1.6
DX12	D	8	348.8	44.5	8.5	73.3	330.9	0				
DX15	D	7	333.6	65.5	7.2	69.6	54.1	0				
DX19	C	5	325.0	36.5	23.5			0				
DX20	D	9	4.5	64.3	3.8	83.1	140.6	0				
DX21	A	6	6.7	43.9	2.7	74.6	270.4	1	31.6	6.55	5.46	−0.7

Site, site ID; Ms-T type, classification of Ms-T curves; N_d, number of the specimens used for the calculation of palaeodirection; Dec, Inc, α_{95}, paleodirection and its 95 per cent confidence circle; P_{Lat}, P_{Long}, latitude and longitude of the virtual geomagnetic pole; N_F, number of the specimens used for the calculation of site-mean paleointensity; F, site-mean palaeointensity with its standard deviation; VDM, VADM, virtual dipole moment and virtual axial dipole moment with associated standard deviations; ΔAIC_{min}, minimum AIC values for the individual sites. Note that the site-mean paleointensity of the site DX04 is calculated without the result of DX04-15-1m as it is regarded as an outlier at the 95% level.

in 9 samples. They show a single phase of Ti-poor titano-magnetite with good reversibility during the heating and cooling cycle, usually resulting in T_c (Curie temperature) ~540–570°C. Type B curves were recognized in 2 samples and resembled type A, though a minor phase of Ti-rich titanomagnetite with T_c of ~ 180 or 240°C is superimposed. Type C curves were seen in 6 samples, showing two components of Ti-poor ($T_c \sim$ 520–550°C) and Ti-rich ($T_c \sim$ 130–190°C) phases. Type D curves were found in five samples: Some superparamagnetic behavior is recognized as an offset in M_s/M_{s0} and the Curie temperatures could not be determined.

The hysteresis parameters, saturation magnetization (Ms), remanent saturation magnetization (Mrs), coercivity (Bc) and remanent coercivity (Brc) were measured for 60 small chips from 30 selected paleomagnetic cores. Measurements were conducted on 1–6 chips for each core, using a vibrating sample magnetometer (MicroMag 3900 VSM, Princeton Measurement Corporation) or an alternating gra-

dient force magnetometer (MicroMag 2900 AGFM, PMC). The resultant Day plot (Day *et al.*, 1977; Dunlop, 2002) is shown in Fig. 3. Core-averaged hysteresis parameters are listed in Table 2.

On the Day plot, some of the data points are distributed along SD (single domain) and MD (multi domain) mixing curves of magnetite (Dunlop, 2002) while others are off-set from the curves locating in the PSD (pseudo-single domain) region. This difference probably originates from the difference in the composition of the main magnetic phase: the compositions are thought to be close to Ti-free titanomagnetite (TM0, magnetite) and Ti-rich titanomagnetites (TMx) for the former and the latter samples, respectively. This is because the curves in Fig. 3 are shown for TM0 and they move toward upper-right region with increasing Ti content (x) (Dunlop, 2002). The former and the latter samples correspond to the samples giving Type A (and/or B) and Type C (and/or B) Ms-T curves, respectively.

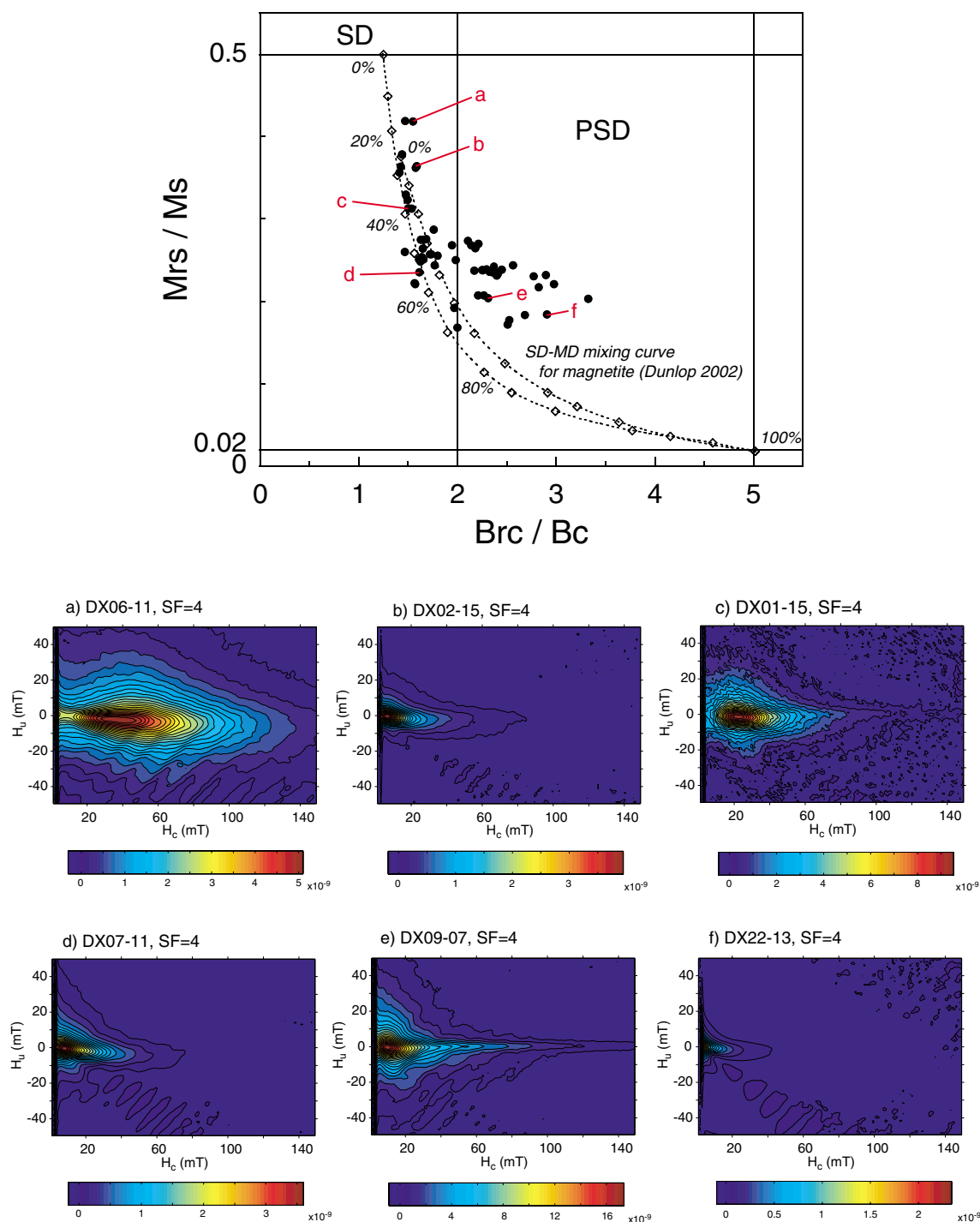The studied samples are considered to be mixtures of

Fig. 3.   Day plot (Day *et al.*, 1977) for the hysteresis parameters of 60 small chips. Some threshold values are modified following Dunlop (2002).
Numbers along mixing curves by Dunlop (2002) indicate % of MD components. FORC diagrams (samples labelled a–f) are also shown.

SD (and/or PSD) and MD particles. This is supported by the FORC (first-order reversal curve; Roberts *et al.*, 2000) measurements, which were performed using the AGFM on specimens from the same 30 selected cores. Figure 3(a)–(f) are representative FORC diagrams. SD-like contributions are clearly recognized by the number of closing contours in all the diagrams (Fig. 3(a)–(f)). MD-like contributions (non-closing contours with relatively low Bc) appear to increase going from sample a (DX06-11) to f (DX22-13), upper-left to lower-right regions in the Day plot (Fig. 3).

In summary, the main remanence carriers in the samples

studied are titanomagnetites with different Ti content (∼ TM0–TM60). They are considered to be mixtures of SD (and/or PSD) and MD particles.

4.   Paleodirections

Stepwise thermal demagnetization (ThD) and alternating field demagnetization (AFD) were conducted on a total of 207 specimens, by using a thermal demagnetizer (TDS-1, Natsuhara-Giken), spinner magnetometers (ASPIN-A and SMD-88, Natsuhara-Giken), and an automatic spinner magnetometer and AF demagnetizer system (Dspin-2, Natsuha-

Table 2. Results of the DHT and LTD-DHT Shaw experiments.

Sample ID	NRM$_0$	ARM0$_0$	B$_{rc}$/B$_c$	M$_{rs}$/M$_s$	LTD (%)	First heating					Second heating					F$_L$ (µT)	F (µT)	ΔAIC
						H$_L$	slope$_{A1}$	slope$_N$	f$_N$	r$_N$	H$_L$	slope$_{A2}$	slope$_T$	f$_T$	r$_T$			
<eastern subgroup>																		
DX01 (N/N0 = 5/9)																		
DX01-03-2L	110	97.0			7.5	12	0.802	0.944	0.825	0.999	20	1.03	1.03	0.806	0.999	15.0	14.2	0.6
DX01-07-2L	71.3	71.2			8.2	12	0.842	0.849	0.918	0.998	22	1.04	1.05	0.741	0.999	15.0	12.7	41.3
DX01-11-2L	124	95.7			13.6	12	0.737	1.02	0.751	0.999	0	0.956	1.04	0.994	0.998	20.0	20.5	17.3
DX01-15-3L	95.7	88.6	1.478	0.3418	7.7	25	0.816	0.595	0.628	0.999	0	0.985	1.01	1.00	0.999	30.0	17.9	−2.0
DX01-17-2	88.0	147				5	0.974	0.252	1.00	0.998	0	1.14	1.00	1.00	0.998	50.0	12.6	30.9
DX03 (N/N0 = 3/6)																		
DX03-05-2L	94.4	66.5	1.478	0.3294	10.0	22	0.731	0.715	0.653	0.999	0	0.977	1.04	0.990	1.00	20.0	14.3	−1.3
DX03-07-2L	66.8	64.1			9.3	22	0.678	0.904	0.629	0.999	0	0.996	1.04	0.996	1.00	15.0	13.6	7.3
DX03-11-1	68.2	131				25	0.668	0.184	0.436	0.998	25	0.892	1.02	0.830	0.999	50.0	9.20	1.3
DX04 (N/N0 = 5/7)																		
DX04-01-2L	97.9	76.7			13.3	22	0.632	1.29	0.470	0.999	0	0.992	1.03	0.998	1.00	15.0	19.4	−1.0
DX04-05-2L	89.7	69.1			8.3	16	0.811	0.792	0.838	0.999	0	0.981	1.03	1.00	1.00	20.0	15.8	0.9
DX04-07-2L	126	91.1			11.2	10	0.683	0.880	0.831	0.995	0	0.984	1.02	1.00	1.00	20.0	17.6	3.5
DX04-11-2L	70.4	61.7	1.497	0.3233	12.4	4	0.749	0.739	0.976	0.998	0	0.996	1.03	0.995	0.999	20.0	14.8	14.5
DX04-15-1m	56.0	110				25	0.626	0.193	0.567	0.998	10	0.900	1.01	0.981	0.997	50.0	9.65	3.3
DX18 (N/N0 = 3/7)																		
DX18-03-2L	104	71.0			12.4	18	0.561	1.07	0.609	0.997	0	0.966	1.02	1.00	1.00	20.0	21.3	8.1
DX18-05-3L	164	86.4			12.0	10	0.685	0.791	0.599	0.999	0	0.988	1.01	0.999	1.00	20.0	15.8	9.3
DX18-11-1L	108	60.8	2.405	0.2356	12.3	8	0.517	1.00	0.578	0.998	0	0.982	0.974	0.996	0.999	20.0	20.1	25.5
DX02 (N/N0 = 5/7)																		
DX02-03-2L	38.5	76.8			9.4	8	0.916	0.420	0.990	0.998	0	1.02	1.03	1.00	1.00	15.0	6.30	−2.0
DX02-05-2L	76.5	102			4.8	6	0.978	0.419	1.00	0.996	0	0.985	1.00	1.00	0.999	20.0	8.38	23.8
DX02-07-3L	35.8	75.0			10.2	10	0.754	0.309	0.902	0.998	0	1.00	1.03	1.00	1.00	15.0	4.64	11.1
DX02-11-2L	58.3	102			8.4	10	0.804	0.436	0.876	0.998	26	1.01	1.05	0.800	0.999	15.0	6.54	4.6
DX02-15-1L	106	146	1.589	0.3640	6.1	4	0.861	0.406	0.879	0.998	16	0.966	0.995	0.969	0.999	20.0	8.12	−1.8
DX05 (N/N0 = 2/8)																		
DX05-03-2L	257	263	1.567	0.2221	12.0	4	0.892	0.586	0.827	0.995	4	0.736	1.05	0.822	0.999	20.0	11.7	1.9
DX05-15-2	213	510				10	0.513	0.212	0.401	0.999	30	1.30	0.978	0.530	0.995	50.0	10.6	−1.9
DX06 (N/N0 = 7/12)																		
DX06-01-2	142	184	1.759	0.2869		20	0.667	1.10	0.447	0.999	15	0.827	0.978	0.749	1.00	20.0	21.9	1.3
DX06-07-2	305	362				35	1.20	1.80	0.458	0.997	15	1.05	0.950	0.717	1.00	20.0	36.1	22.0
DX06-09-2	218	364				35	0.589	0.764	0.497	1.00	20	1.07	0.955	0.922	1.00	20.0	15.3	−2.0
DX06-13-1	153	188	1.473	0.4189		30	0.949	0.745	0.683	0.999	0	1.06	1.03	1.00	1.00	20.0	14.9	−2.0

Sample ID	NRM_0	$ARM0_0$	B_{rc}/B_c	M_{rs}/M_s	LTD (%)	First heating					Second heating					F_L (µT)	F (µT)	ΔAIC
						H_L	$slope_{A1}$	$slope_N$	f_N	r_N	H_L	$slope_{A2}$	$slope_T$	f_T	r_T			
DX06-13-3L	176	94.2	1.473	0.4189	3.2	2	1.02	0.870	0.968	0.998	0	0.974	0.974	1.00	0.999	25.0	21.8	9.0
DX06-15-1	178	156	1.578	0.3618		10	0.907	1.23	0.962	1.00	0	1.01	1.05	1.00	0.997	20.0	24.6	−1.7
DX06-15-2L	196	87.0	1.578	0.3618	5.4	4	1.03	1.10	0.962	0.998	0	0.956	1.01	0.990	0.999	25.0	27.6	11.1
DX07 (N/N0 = 7/8)																		
DX07-01-1L	168	145			14.2	0	0.593	1.03	1.00	0.995	4	0.940	1.04	0.928	0.996	15.0	15.5	−0.4
DX07-07-1	119	307	1.726	0.2589		15	0.443	0.285	0.325	0.999	15	0.690	0.999	0.680	0.998	50.0	14.3	−1.3
DX07-07-3L	128	114	1.726	0.2589	12.4	0	0.842	0.990	0.990	0.999	0	1.01	1.01	0.991	0.999	15.0	14.9	5.6
DX07-11-1	131	311	1.616	0.2352		5	0.615	0.250	0.735	0.999	35	0.832	1.02	0.637	0.999	50.0	12.5	8.8
DX07-11-3L	126	142	1.616	0.2352	13.0	0	0.869	0.767	1.00	0.998	0	0.973	1.02	0.984	0.998	15.0	11.5	−1.9
DX07-13-3L	94.3	114			17.8	4	0.640	0.592	0.963	0.995	8	1.02	1.01	0.918	0.999	20.0	11.8	−0.3
DX07-15-1	98.9	195				10	0.764	0.738	0.728	0.999	30	1.17	1.04	0.641	0.999	20.0	14.8	−0.3
DX08 (N/N0 = 5/7)																		
DX08-03-3L	163	119	1.468	0.2598	8.9	8	0.812	0.888	0.836	0.998	0	0.969	1.04	0.995	0.997	20.0	17.8	−0.7
DX08-07-1	179	351				0	0.908	0.380	1.00	0.998	25	0.649	1.01	0.487	0.999	50.0	19.0	0.3
DX08-09-1	206	324				10	0.574	0.325	0.666	0.997	40	0.872	0.952	0.574	1.00	50.0	16.3	25.9
DX08-13-2	130	247				15	0.291	1.03	0.277	0.999	25	0.816	0.988	0.606	1.00	20.0	20.6	1.1
DX08-15-2	183	315				10	0.659	0.781	0.618	0.999	10	0.942	0.999	0.961	0.999	20.0	15.6	−1.8
DX09 (N/N0 = 4/7)																		
DX09-07-1	105	137	2.265	0.2060		20	0.684	0.397	0.431	0.998	0	1.01	1.01	1.00	0.999	50.0	19.9	6.9
DX09-07-3L	108	90.2	2.265	0.2060	8.8	20	0.821	0.891	0.569	0.996	0	0.990	0.982	1.00	1.00	20.0	17.8	14.1
DX09-13-2L	64.0	64.4	1.634	0.2668	11.8	22	0.569	0.900	0.514	0.996	0	0.954	0.972	1.00	0.999	20.0	18.0	20.4
DX09-15-2	82.2	116				25	0.651	0.877	0.381	0.997	0	1.04	0.969	1.00	0.998	20.0	17.5	16.5
DX17 (N/N0 = 3/5)																		
DX17-05-2	291	347				10	0.728	0.853	0.398	0.997	25	0.897	0.984	0.742	0.999	20.0	17.1	1.7
DX17-09-1	209	402				15	0.665	0.283	0.300	0.998	30	0.517	0.961	0.411	0.997	50.0	14.2	12.8
DX17-15-2L	160	164	2.267	0.2372	16.6	6	0.483	0.503	0.695	0.997	16	0.985	1.04	0.934	0.997	25.0	12.6	9.7
<western subgroup>																		
DX13 (N/N0 = 4/5)																		
DX13-05-1	241	174				25	0.922	1.02	0.195	0.999	15	0.694	0.960	0.507	0.998	50.0	51.2	−2.0
DX13-07-3L	315	95.0	1.576	0.2206	6.3	8	1.45	1.25	0.561	0.996	4	0.779	0.969	0.779	0.995	50.0	62.4	34.6
DX13-11-1L	198	82.7	2.001	0.1682	16.0	8	1.12	0.758	0.673	0.997	8	0.737	1.03	0.676	0.999	50.0	37.9	−1.8
DX13-13-1	296	197				15	0.784	1.17	0.297	0.999	25	1.09	0.983	0.445	0.996	50.0	58.4	−1.2
DX14 (N/N0 = 1/2)																		
DX14-13-3L	506	323			16.0	10	0.638	1.06	0.567	0.996	6	0.882	0.958	0.728	0.999	25.0	26.6	13.3
DX16 (N/N0 = 1/5)																		

Sample ID	NRM$_0$	ARM0$_0$	B$_{rc}$/B$_c$	M$_{rs}$/M$_s$	LTD (%)	First heating					Second heating					F$_L$ (μT)	F (μT)	ΔAIC
						H$_L$	slope$_{A1}$	slope$_N$	f$_N$	r$_N$	H$_L$	slope$_{A2}$	slope$_T$	f$_T$	r$_T$			
DX16-01-3L	552	233			14.5	12	0.833	2.12	0.605	0.999	0	0.971	0.980	1.00	1.00	25.0	53.0	21.1
DX22 (N/N0 = 2/4)																		
DX22-13-1L	477	245	3.044	0.2064	18.8	10	0.856	1.82	0.711	0.997	8	0.935	0.951	0.755	0.999	25.0	45.4	32.5
DX22-15-1L	722	249			17.1	10	0.859	1.79	0.764	0.997	4	0.919	0.986	0.830	1.00	25.0	44.8	60.2
DX10 (N/N0 = 5/6)																		
DX10-03-1L	363	168			15.8	8	0.670	1.24	0.827	0.995	0	0.987	1.02	1.00	0.998	25.0	31.0	29.1
DX10-07-2	221	410				10	0.624	1.11	0.641	0.999	25	0.871	1.02	0.788	1.00	20.0	22.2	−1.9
DX10-09-1L	191	144			11.0	10	0.688	0.823	0.608	0.997	28	1.00	1.04	0.872	0.997	25.0	20.6	−0.6
DX10-13-1	196	319	1.972	0.1920		10	0.834	0.514	0.843	0.998	30	0.591	0.964	0.610	1.00	50.0	25.7	7.1
DX10-15-2	385	344				15	0.630	1.86	0.684	0.999	20	0.972	0.996	0.858	0.998	20.0	37.2	−0.3
DX11 (N/N0 = 3/4)																		
DX11-07-3L	183	92.5			12.5	12	0.533	1.48	0.511	0.996	4	0.821	1.02	0.941	0.999	25.0	36.9	1.1
DX11-11-2L	256	137	2.182	0.2645	9.3	12	0.763	1.20	0.584	0.996	0	0.837	1.02	0.991	0.999	25.0	29.9	−1.6
DX11-15-2L	182	92.4			8.6	8	0.515	1.07	0.669	0.998	0	0.833	1.01	0.977	0.999	25.0	26.8	0.8
DX12 (N/N0 = 0/1)																		
DX19 (N/N0 = 0/1)																		
DX20 (N/N0 = 0/4)																		
DX21 (N/N0 = 1/2)																		
DX21-03-1L	274	149	2.859	0.2225	9.5	0	*1.02*	*1.26*	0.992	1.00	0	0.986	0.980	1.00	1.00	25.0	31.6	−0.7

NRM$_0$, ARM0$_0$, initial NRM and ARM0 intensity after LTD (10^{-5} Am^2/kg); B$_{rc}$/B$_c$, M$_{rs}$/M$_s$, core-averaged ratios of remanent coercivity and remanent saturation magnetization; LTD, LT demagnetized fraction of ARM0 (%); H$_L$, the lowest coercivity force taken for the linear segments; slope$_{A1}$, slope$_{A2}$, slopes of ARM spectra ($\geq$ H$_L$) in the ARM0-ARM1 and ARM1-ARM2 diagrams; slope$_T$, slopes of the linear segments in the NRM-TRM1* and TRM1-TRM2* diagrams; f$_N$, f$_T$, NRM and TRM1 fractions of the linear NRM-TRM1* and TRM1-TRM2* segments; r$_N$, r$_T$, correlation coefficients of the linear NRM-TRM1* and TRM1-TRM2* segments; F$_L$, laboratory induced DC field for TRM1 and TRM2; F, calculated paleointensity; ΔAIC, AIC difference between linear and quadratic fit (Yamamoto and Tsunakawa, 2005). The LTD-DHT Shaw method was conducted on specimens with suffix 'L' whereas the DHT Shaw method on others. Note that only successful results are indicated, and that the result of DX04-15-1m is excluded as an outlier (at the 95% level) in the calculation of the site-mean for DX04.
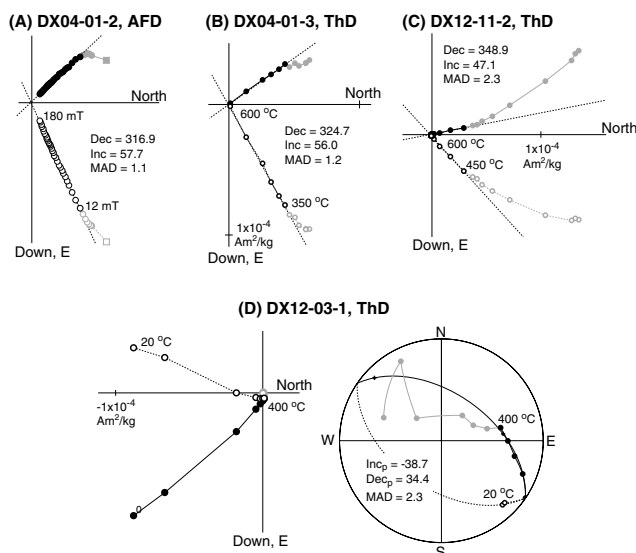
Fig. 4. Representative orthogonal vector plots of (A) ThD and (B) AFD except for the sites DX12 and DX19. In the site DX12, linear analysis was only possible for two specimens (C) and rest six specimens showed demagnetization behaviors trending great circles (D). Closed and open circles indicate horizontal and vertical projections, respectively. In (D), inclination (Inc_p), declination (Dec_p) and maximum angular deviation (MAD) of a best-fit great circle are indicated.

ra-Giken; Kono *et al.*, 1984, 1997). Except for two sites (DX12 and DX19), primary remanences were isolated from natural remanent magnetizations (NRMs) after removal of secondary components by about 450°C or 25 mT. Most of the demagnetization results yielded primary components with MAD (maximum angular deviation; Kirschvink, 1980) ≤ 5.0° (Fig. 4(A) and (B)). Determinations of site-mean paleodirections were straightforward for these sites.

In the site DX12, linear analysis was only possible for two specimens (Fig. 4(C)). The remaining six specimens suffered from large secondary components. However, because these specimens showed good remagnetization circles (Fig. 4(D)), the site-mean paleodirection was successfully obtained by the combined analysis of linear components and remagnetization circles of McFadden and McElhinny (1988).

In the site DX19, no results were available for linear analyses: all eight specimens showed large secondary components during demagnetization. These results could be fitted to remagnetization circles, but they give a mean direction of α_{95} of 23.5° (N=5) which is not acceptable.

All the resultant paleodirections show normal Brunhes Chron polarity without any indication of geomagnetic excursions. VGP (virtual geomagnetic pole) latitudes range between 53.2°N and 83.1°N. The site-mean paleodirections are listed in Table 1.

5. Paleointensity

Paleointensity measurements were performed by three different methods: (1) the double heating technique of the Shaw method (DHT Shaw method; Tsunakawa and Shaw, 1994) and the DHT Shaw method with low temperature demagnetization (LTD-DHT Shaw method; Tsunakawa and

Shaw, 1994; Yamamoto *et al.*, 2003), (2) the Thellier method with Coe's modification (Thellier and Thellier, 1959; Coe *et al.*, 1978) and (3) the microwave Thellier method (Shaw *et al.*, 1996; Hill and Shaw, 1999). We conducted the method of (1) on 119 specimens while those of (2) and (3) were applied to 29 and 73 specimens, respectively. Note that we categorize the DHT and the LTD-DHT Shaw methods as a one method because they are very similar except for some points (see Section 5.1).

5.1 DHT and LTD-DHT Shaw methods

The DHT and LTD-DHT Shaw methods were applied to 49 and 70 specimens, respectively. The former experiment was carried out at the paleomagnetism laboratory in the Tokyo Institute of Technology, Japan, whereas the latter was performed at the Geological Survey of Japan, AIST.

In the DHT Shaw experiment, the samples were subjected to progressive AF demagnetization at 5–10 mT steps up to 120 mT, using an AF demagnetizer (DEM8601C, Natsuhara-Giken). Remanences were measured with an ASPIN-A spinner magnetometer (Natsuhara-Giken). Laboratory TRM (thermal remanent magnetization) was imparted by heating the samples in air to a maximum temperature of 610°C in a constant magnetic field (20.0–50.0 μT). Hold time at the temperature was 10 (first heating) and 20 minutes (second heating), and entire heating-cooling cycle took about two hours. The field was applied throughout the cycle. Anhysteretic remanent magnetization (ARM) was given using a 100.0 μT biasing field with a peak AF of 120 mT.

In the LTD-DHT Shaw experiment, progressive AF demagnetization was applied in 2–10 mT steps up to 180 mT, using an automatic spinner magnetometer and AF demagnetizer system (Dspin-2, Natsuhara-Giken: Kono *et al.*, 1984, 1997). Remanences were simultaneously measured by the system. TRM was imparted by heating the samples in vacuum (10–10^2 Pa) to a maximum temperature of 610°C in a constant magnetic field (15.0–50.0 μT). Hold time at the maximum temperature was 24 (first heating) and 48 minutes (second heating), and entire heating-cooling cycle took about four hours. The field was applied throughout the cycle. ARM was given using a 50.0 μT biasing field with a maximum AF of 180 mT. Prior to progressive AF demagnetization of the NRM, TRM and ARM, samples underwent low temperature demagnetization (LTD: Ozima *et al.*, 1964; Heider *et al.*, 1992). They were soaked in liquid nitrogen for 10 minutes and then taken out of the dewar and left at room temperature for an hour. The liquid nitrogen was contained in a non-magnetic dewar and the complete cooling/warming cycle was carried out in zero field.

NRM-TRM1* and TRM1-TRM2* diagrams were constructed from the experimental results where TRM1* and TRM2* denote TRM1 and TRM2 corrected using the technique of Rolph and Shaw (1985). These corrections are based on the assumption that changes in the coercivity spectra of the TRM will also be reflected in the spectra of the ARM. Similar to previous studies (Yamamoto *et al.*, 2003; Mochizuki *et al.*, 2004, 2006; Oishi *et al.*, 2005; Yamamoto and Tsunakawa, 2005), the results are judged by the following quantitative selection criteria.
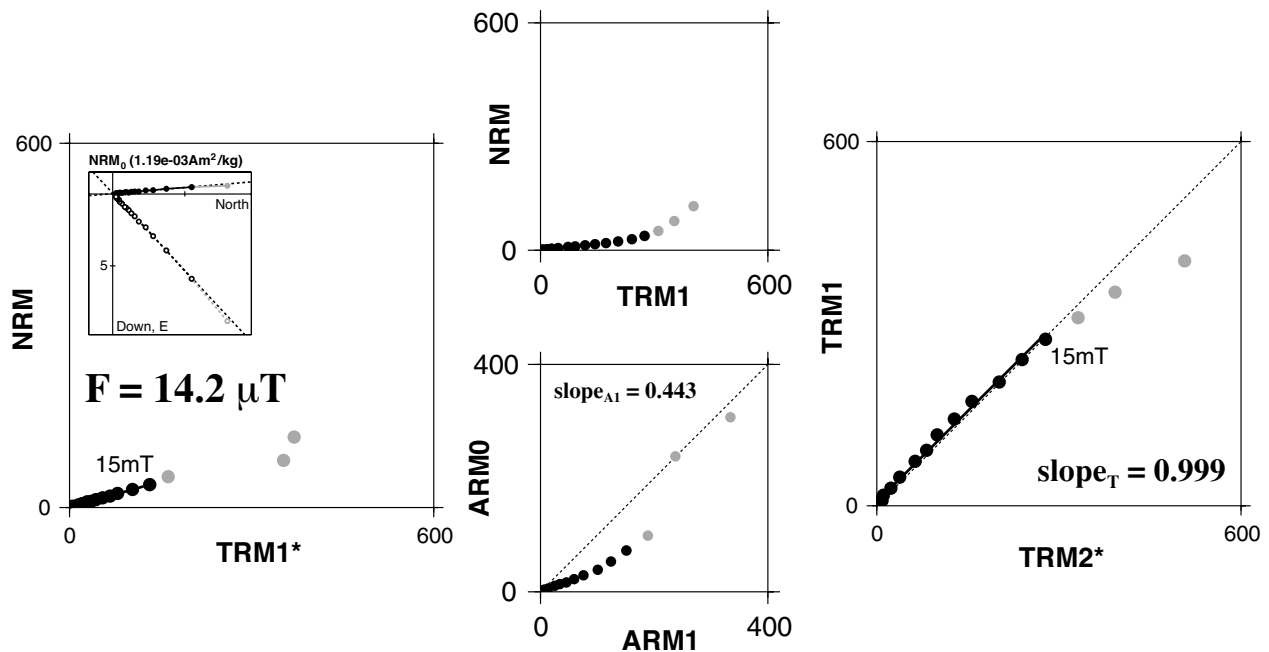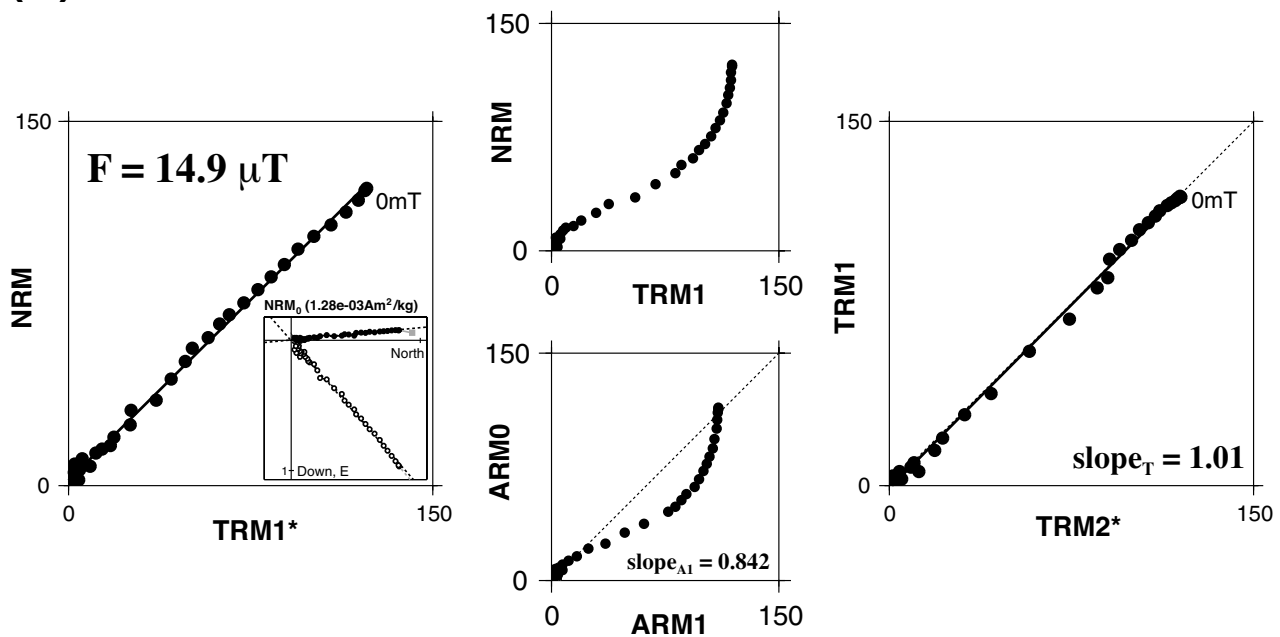
(A) DX07-07-1

(B) DX07-07-3

Fig. 5. Representative successful results of the DHT and LTD-DHT Shaw experiments. (A) DX07-07-1 by the DHT Shaw method, and (b) DX07-07-3 by the LTD-DHT Shaw method. These results were obtained from the same paleomagnetic core. The left three diagrams illustrate results from the first laboratory heating while the right one is from the second heating. Linear portions consist of closed symbols. Orthogonal vector plots of AFD on NRM are also shown as insets, where closed and open symbols indicate projections onto horizontal and vertical planes, respectively (squares are NRM before LTD). Units are in 10^{-5} A m^2/kg.

(1) A stable primary component of remanence is recognized in the orthogonal plot obtained from AF demagnetization of the NRM.

(2) A linear portion should exist in the NRM-TRM1* diagram which is not less than 15% of the original NRM intensity ($f_N \geq 0.15$), and the correlation coefficient should be larger than 0.995 ($r_N \geq 0.995$).

(3) The linear portion ($f_T \geq 0.15$ and $r_T \geq 0.995$)

should also exist in the TRM1-TRM2* diagram. The slope must be unity within experimental errors ($1.05 \geq$ Slope$_T \geq 0.95$) as proof of the validity of the ARM correction.

These selection criteria were satisfied by 27 DHT Shaw and 39 LTD-DHT Shaw results. Representative successful results are shown in Fig. 5 and all individual results are

(A) DX06-05-3
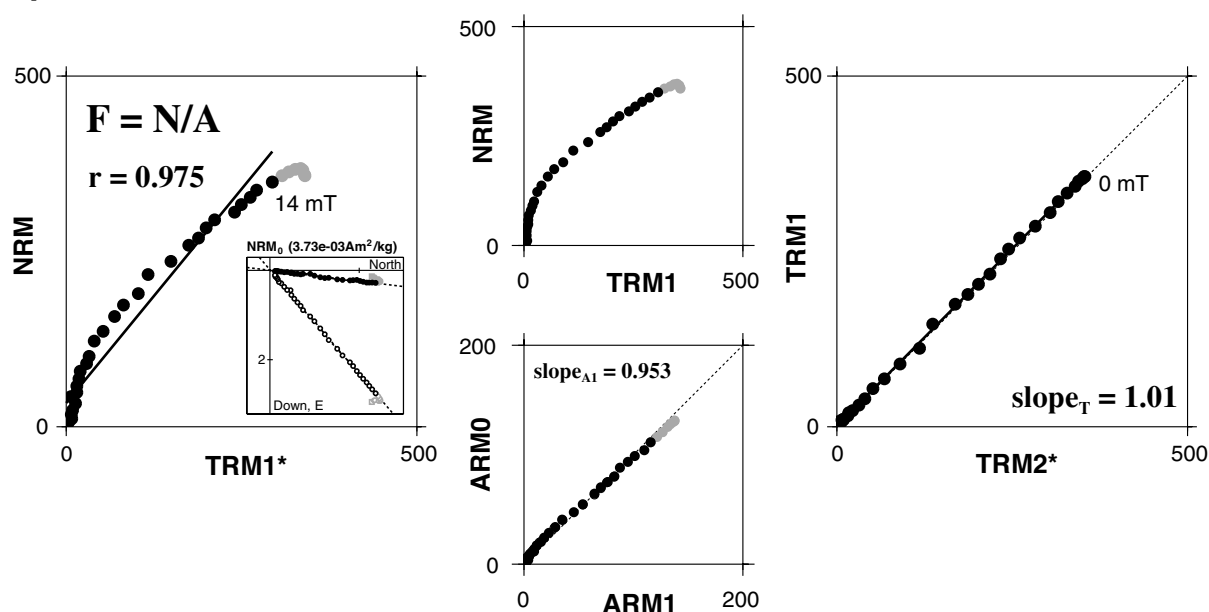
(B) DX05-11-1
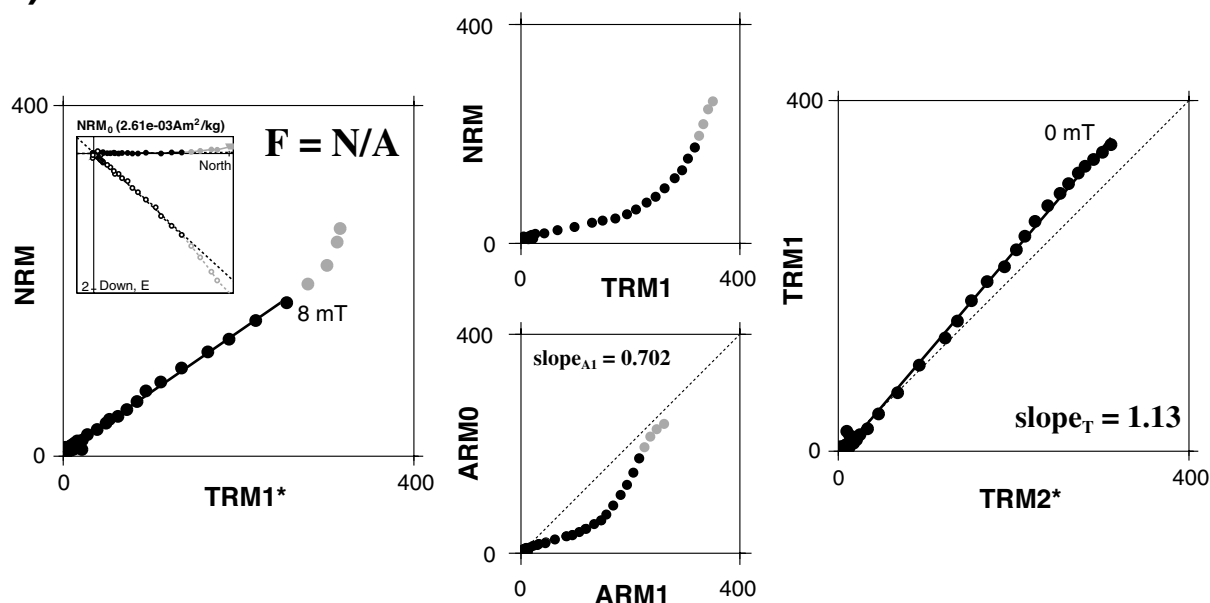
Fig. 6. Examples of the unsuccessful results of the DHT and LTD-DHT Shaw experiments. The reasons for the rejection are (A) a low correlation coefficient in the NRM-TRM1* diagram ($r_N < 0.995$) and (B) a non-unity slope in the TRM1-TRM2* diagram ($Slope_T < 0.95$ or $1.05 < Slope_T$).

listed in Table 2. Successful paleointensity results range from 4.64 μT to 62.4 μT. Because the present field intensity at the site location is estimated to be 54.8 μT (IGRF-10; IAGA Division V Working Group VMOD, 2005), the obtained values are generally lower than the present day field. Unsuccessful results were rejected mainly due to lower values of the correlation coefficients in the NRM-TRM1* diagrams ($r_N < 0.995$; Fig. 6(A)) or non-unity slopes in the TRM1-TRM2* diagrams ($1.05 < Slope_T$; Fig. 6(B)).

79% of the successful results yielded ΔAIC values (Yamamoto and Tsunakawa, 2005) less than 15.0 (Table 2). The ΔAIC value is a measure of the preference between linear and quadratic fits in the NRM-TRM1* diagram. In Ya-

mamoto and Tsunakawa (2005), they tentatively concluded that ΔAIC exceeding ~ 15 is possibly a sign of low quality paleointensity based on their Society Islands dataset. Although their conclusion may not be applicable to the present results (because they compose a different dataset), they are generally considered to be of good quality.

In the LTD-DHT Shaw experiment, the samples exhibited about 5–20% loss of ARM0 by LTD (Table 2). This means that laboratory induced ARMs (before laboratory heating) were demagnetized by about 5–20% by LTD, implying that there is a certain amount of MD-like contribution in the samples. The hysteresis and FORC measurements also support this (Section 3). This may explain the

(A)

(B)   (C)
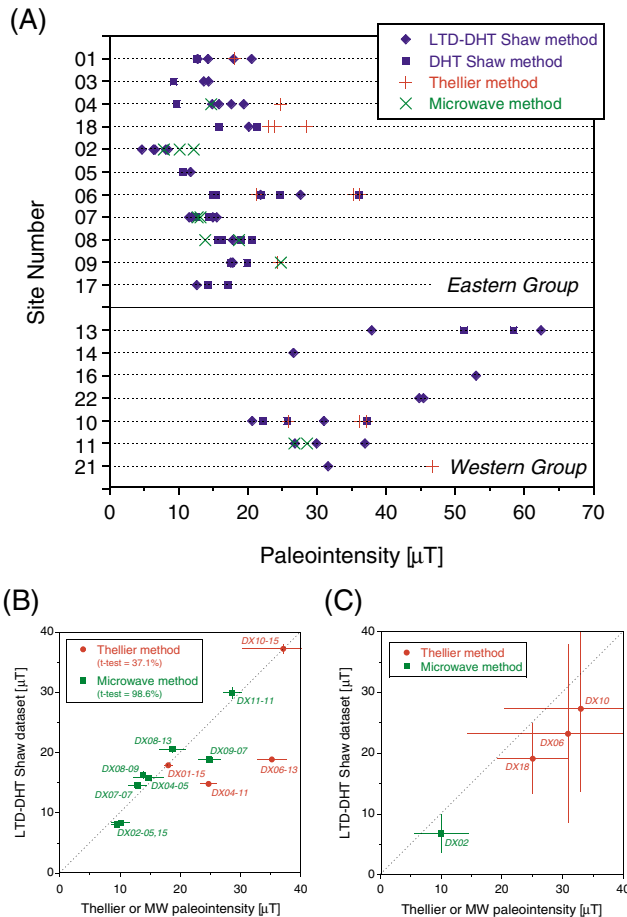
Fig. 7. (A) Paleointensity results plotted against each sampling site. Numbers in the vertical axis indicate site numbers (e.g. 01 means the site DX01). Blue diamonds, blue squares, red cross and green christcross are results by the LTD-DHT Shaw method, the DHT Shaw method, the Thellier method and the microwave Thellier method, respectively. (B) Comparisons of paleointensities obtained from same paleomagnetic cores. The Thellier (red circles) and the microwave Thellier paleointensities (green squares) are plotted against the LTD-DHT Shaw dataset. Error bars indicate two standard errors. (C) Comparisons of the site-mean paleointensities obtained from the four sites. The Thellier (red circles) and the microwave Thellier site-means (green squares) are plotted against the LTD-DHT Shaw site-means. Error bars indicate two standard deviations.

differences between the DHT and the LTD-DHT Shaw results because the former were obtained without any LTD pre-treatments. However, consistent DHT and LTD-DHT Shaw paleointensities are observed from several pairs of sister specimens (e.g. Fig. 5). In a comparison of the results at the site-level (blue squares and diamonds in Fig. 7(A)), no systematic differences between the DHT and the LTD-DHT Shaw paleointensities were observed. In later discussions, we therefore treat both sets of paleointensities as the same "LTD-DHT Shaw dataset". Site-mean paleointensities of the LTD-DHT Shaw dataset are summarized in Table 1.

5.2 Thellier method

The Thellier method with Coe's modification (Thellier and Thelleir, 1959; Coe *et al.*, 1978) was applied to 29 specimens. The specimens were subjected to a series of zero-field and in-field heating-cooling cycles at 20–50°C intervals up to 600°C. In the in-field cycles, the field was applied throughout the cycles. Partial TRM (pTRM) checks

were made at every one or two temperature steps for all specimens while the pTRM-tail check (Shcherbakova *et al.*, 2000; Riisager and Riisager, 2001) was conducted on one specimen (DX01-15-1). The heating and cooling were carried out in air in about two hours (hold time at maximum temperatures were 15–20 minutes) using TDS-1 (Natsuhara Giken) or MMTD-18 (Magnetic Measurements) electric furnaces. Remanent magnetizations were measured using spinner magnetometers (SMM-85 or SMD-88, Natsuhara Giken).

The results are analyzed using Arai plots (Nagata *et al.*, 1963). Similar to the study by Tanaka *et al.* (2007), they are judged on various quality parameters (Coe *et al.*, 1978; Selkin and Tauxe, 2000; Kissel and Laj, 2004). Acceptance criteria are as follows.

(1) The Arai plot should have a linear portion that includes at least four data points ($N \geq 4$) with a correlation coefficient -r and a NRM fraction f_N not less than 0.970 and 0.35, respectively (-r $\geq$ 0.970 and $f_N \geq$ 0.35).

(2) The linear portion should have positive pTRM checks that are judged by pTRM differences between the first and repeat steps with the field applied. If the differences normalized by the length of the linear segment (DRATs) are smaller than 7% (DRAT < 7%) and their accumulation over the selected temperature interval (CDRAT) are smaller than 10% (CDRAT < 10%), then pTRM checks are considered to be positive.

(3) The remanence vector of the zero-field step data which constitutes the selected linear segment should show a reasonable decrease toward the origin on the orthogonal plot. This is judged by the difference angle α and a deviation *dev* of Tanaka and Kobayashi (2003), which should be smaller than 10° and 10%, respectively (α < 10. and *dev* < 10%).

Successful results were obtained from 16 specimens. They are summarized in Table 3. Except for three results, the resultant Arai plots give single slopes (Fig. 8(A) and (B)). Paleointensity calculations are straightforward and range between 18.0 μT and 53.8 μT. As with the LTD-DHT Shaw dataset, they are generally weak compared to the present day field strength at the site (54.8 μT).

Problematic behavior is seen in the three results: high paleointensities are obtained from low temperature intervals (Fig. 8(C)) whereas low paleointensities are obtained from high temperature intervals (Fig. 8(D)). The quality factor for these results is similar to the quality factor from samples with single slopes in the Arai plots (5.6–16.8 for the former and 2.1–39.0 for the latter; Table 3). Two-sloped Arai plots have been often reported in recent studies (e.g. Yamamoto and Tsunakawa, 2005). Possible reasons are (1) large amount of MD-like contribution (e.g. Levi, 1977; Xu and Dunlop, 2004), (2) non-detectable cumulative laboratory alteration (e.g. Coe *et al.*, 1984; Mochizuki *et al.*, 2004), (3) acquisition of thermochemical remanent magnetizations (TCRM) during natural cooling (e.g. Yamamoto *et al.*, 2003; Yamamoto, 2006), and (4) differences in cooling-rate between natural and laboratory conditions (e.g. Fox and Aitken, 1980; Chauvin *et al.*, 2005; Bowles *et al.*, 2005; Morales *et al.*, 2006). Because the rock magnetic experi-

Table 3. Results of the Thellier experiment.

Sample ID	NRM_0 $(10^{-5}$ A m^2/kg)	T_1–T_2 (°C)	N	-r	q	f	α (°)	dev (%)	slope	F_L (μT)	F (μT)
<eastern subgroup>											
DX01 (N/N0 = 2/2)											
DX01-15-1	90.9	20–540	15	0.998	39.0	0.821	2.8	3.8	0.720±0.013	25.0	18.0
DX01-19-1	94.3	150–500	10	0.997	14.4	0.457	2.7	3.5	0.540±0.015	50.0	27.0
		520–600	5	0.996	9.2	0.668	1.2	0.6	0.184±0.009	50.0	9.20
DX03 (N/N0 = 0/1)											
DX04 (N/N0 = 1/1)											
DX04-11-1	80.3	400–520	6	0.999	12.4	0.419	5.9	5.9	0.494±0.013	50.0	24.7
DX18 (N/N0 = 4/5)											
DX18-01-2	97.0	100–520	12	0.999	33.4	0.570	1.8	2.3	0.568±0.009	50.0	28.4
DX18-09-1	82.1	400–520	6	0.999	12.2	0.374	5.6	7.0	0.457±0.011	50.0	22.9
DX18-13-1	159	250–520	9	0.995	8.4	0.375	3.2	1.6	0.616±0.023	50.0	30.8
		540–600	4	0.997	5.6	0.532	0.4	0.2	0.249±0.014	50.0	12.5
DX18-15-2	61.6	20–450	10	0.997	11.7	0.383	4.0	6.0	0.477±0.013	50.0	23.9
DX02 (N/N0 = 0/1)											
DX06 (N/N0 = 4/5)											
DX06-01-3	179	250–500	7	0.996	7.8	0.398	4.8	5.5	3.32±0.14	20.0	66.3
		520–600	5	0.999	16.8	0.608	1.6	1.0	0.826±0.021	20.0	16.5
DX06-05-2	246	500–600	5	0.998	13.8	0.705	1.8	1.3	1.06±0.04	20.0	21.3
DX06-11-2	169	20–500	8	0.999	19.0	0.489	1.9	2.7	1.81±0.04	20.0	36.1
DX06-13-2	178	20–500	8	0.996	11.3	0.501	1.8	2.6	1.76±0.06	20.0	35.2
DX09 (N/N0 = 1/1)											
DX09-11-2	75.0	400–520	6	1.00	23.1	0.417	5.1	5.4	0.485±0.007	50.0	24.3
DX17 (N/N0 = 0/1)											
<western subgroup>											
DX13 (N/N0 = 0/4)											
DX10 (N/N0 = 3/5)											
DX10-01-1	414	200–520	8	0.996	13.1	0.600	1.7	2.1	1.81±0.07	20.0	36.2
DX10-05-3	413	470–560	5	0.999	20.3	0.697	1.2	1.0	1.29±0.33	20.0	25.8
DX10-15-1	348	20–435	6	0.983	3.2	0.399	5.6	7.5	1.85±0.17	20.0	37.1
DX12 (N/N0 = 0/1)											
DX19 (N/N0 = 0/1)											
DX21 (N/N0 = 1/1)											
DX21-07-1	427	20–500	16	0.996	21.9	0.540	1.3	1.8	0.934±0.021	50.0	46.7

NRM_0, initial NRM intensity; T_1–T_2, N, -r, q, f, slope, temperature interval, number of the data points, correlation coefficient, quality factor, NRM fraction, and slope of the linear NRM-TRM portion in the Arai plot; α, dev, difference angle and deviation of the selected NRM component; F_L, laboratory induced DC field for TRM; F, calculated paleointensity. Note that only successful results are indicated.

ments did not suggest a large MD-like contribution (Section 3), reason (1) does not seem to be possible. However, several studies reported concave-up Arai diagrams from samples showing similar hysteresis properties as the present samples, suggesting the existence of a certain amount of MD grains as the possible cause (e.g. Shcherbakov and Scherbakova, 2001; Calvo *et al.*, 2002; Biggin and Thomas, 2003). Also, Biggin (2006) predicted that Thellier experiments with intensive heating steps on samples with SD/MD ratios of 1.0 can result in curved Arai diagrams as Fig. 8(C) and (D). We cannot completely rule out this possibility. The remaining three reasons might be possible but there is no supporting evidence. As suggested by Valet (2003), we

think it is better to omit these three results from the later discussion.

Unsuccessful results mainly originate from the production of chemical remanent magnetization (CRM) during laboratory heating. They give concave-up Arai plots which are easily recognized (Fig. 8(E) and (F)).

5.3 Microwave Thellier method

We used the 14 GHz microwave demagnetizing-remagnetizing system for the paleointensity determination. The system is equipped with an integrated liquid nitrogen SQUID magnetometer to measure the magnetization of the 5 mm diameter mini core samples (Hill *et al.*, 2005). In this study, two methods were used: the perpendicular applied
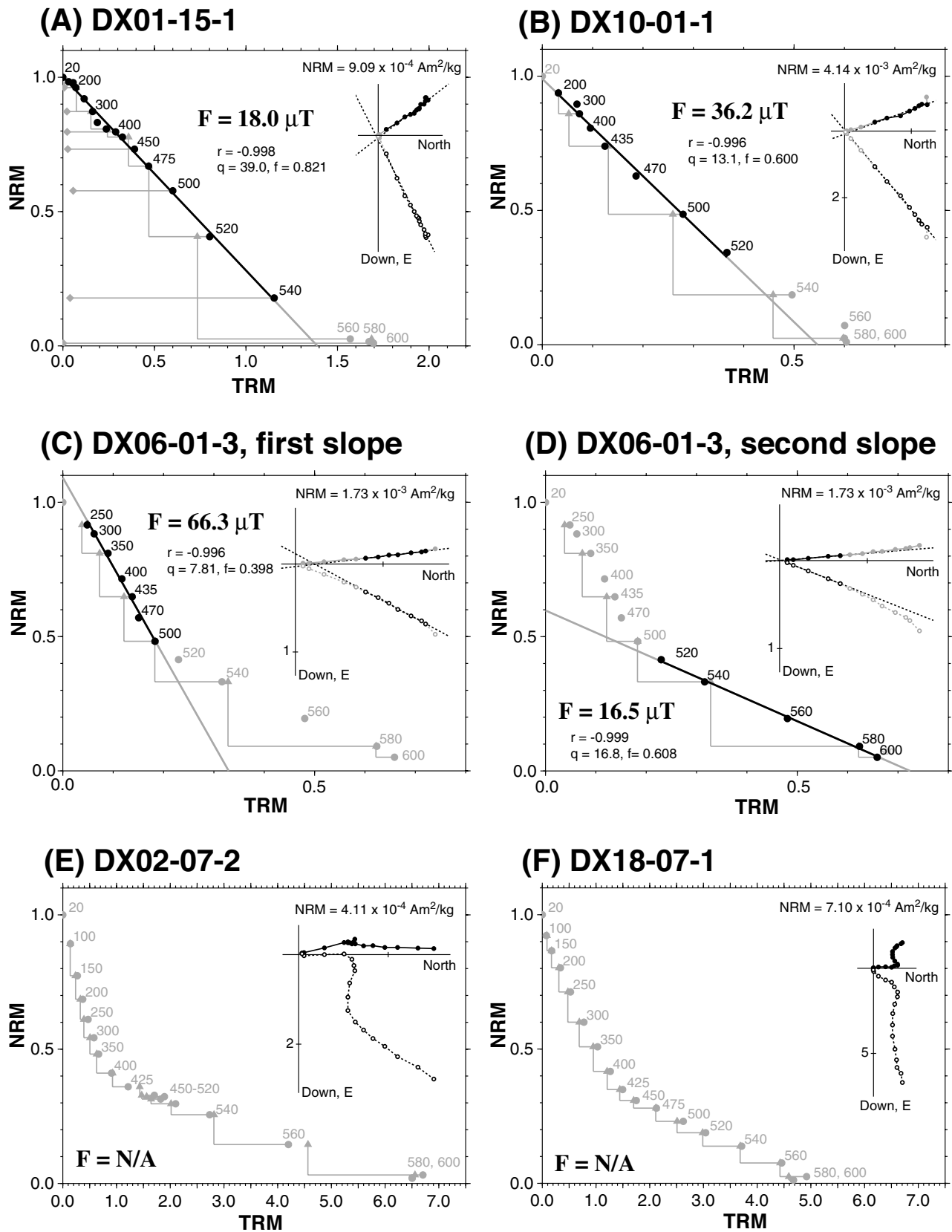
Fig. 8.   Representative Arai plots from the results of the Thellier experiment. (A and B) Examples of the plots giving single slopes (closed diamonds represent results of the pTRM-tail checks). (C and D) Examples of problematic two-sloped behavior. (E and F) Examples of rejected results.

Table 4. Results of the microwave Thellier experiment.

Sample ID	method	P$_1$–P$_2$ (W)	N	-r	q	f	α (°)	dev (%)	slope	F$_L$ (μT)	F (μT)
<eastern subgroup>											
DX04 (N/N0 = 1/5)											
DX04-05-3c	coe	52–71	5	0.990	3.59	0.489	5.4	6.2	0.978±0.081	15.0	14.7
DX18 (N/N0 = 0/11)											
DX02 (N/N0 = 3/5)											
DX02-05-3e	coe	22–33	5	0.991	5.08	0.589	4.3	5.1	0.672±0.051	15.0	10.1
DX02-15a-2c	perp	7–19	7	0.994	7.66	0.466			0.808±0.040	15.0	12.1
DX02-15a-2d	coe	1–22	8	0.984	5.84	0.504	6.3	8.3	0.520±0.038	15.0	7.8
DX05 (N/N0 = 0/5)											
DX07 (N/N0 = 2/5)											
DX07-07-2b	perp	11–40	13	0.980	6.99	0.460			0.874±0.052	15.0	13.1
DX07-07-2c	perp	25–58	8	0.974	4.21	0.457			0.846±0.078	15.0	12.7
DX08 (N/N0 = 3/14)											
DX08-07-2c	coe	7–18	6	0.993	5.08	0.377	1.2	1.4	1.69±0.10	15.0	25.4
		18–50	8	0.996	15.4	0.710	5.8	4.4	0.562±0.022	20.0	11.2
DX08-09-2c	coe	1–25	9	0.999	26.3	0.514	1.8	2.3	0.920±0.016	15.0	13.8
DX08-13-3e	coe	5–19	7	0.992	6.45	0.452	3.3	4.4	1.25±0.07	15.0	18.7
DX09 (N/N0 = 1/8)											
DX09-07-2c	coe	35–71	11	0.995	16.9	0.647	3.2	3.2	1.65±0.06	15.0	24.8
DX17 (N/N0 = 0/7)											
<western subgroup>											
DX13 (N/N0 = 0/2)											
DX10 (N/N0 = 0/3)											
DX11 (N/N0 = 2/8)											
DX11-11-1c	coe	3–70	15	0.996	34.1	0.976	0.7	0.7	1.14±0.03	25.0	28.6
DX11-13-3b	perp	7–26	9	0.997	12.3	0.398			1.07±0.03	25.0	26.7

method, type of applied methods (perpendicular (perp) or double heating (coe)); P$_1$–P$_2$, N, -r, q, f, slope, power interval, number of the data points, correlation coefficient, quality factor, NRM fraction, and slope of the linear NRM-TRM portion in the Arai plot; α, dev, difference angle and deviation of the selected NRM component; F$_L$, laboratory induced DC field for TRM; F, calculated paleointensity. Note that only successful results are indicated.

field method (Kono and Ueno, 1977; Hill and Shaw, 1999) and the double 'heating' method (Coe *et al.*, 1978; Thomas *et al.*, 2004).

The perpendicular method was applied to 51 specimens. The sample is firstly subjected to demagnetization until secondary or viscous overprints are erased. Then the field is applied perpendicular to the isolated NRM direction and remains applied for all remagnetization steps. The double 'heating' method was applied to 22 specimens. A series of zero-field and in-field microwave application cycles were repeated until the remaining NRM is demagnetized to less than 10% of the original. Microwave power applied is between 0–80 W and the application time is set to 5 seconds. Partial T$_M$RM (microwave induced TRM) and pT$_M$RM-tail checks are performed at every two or three remagnetization steps. Details of the experimental procedures can be found in Gratton *et al.* (2005) and Hill *et al.* (2005).

The results are judged by the acceptance criteria described in Section 5.2. Results of the pT$_M$RM-tail checks are not taken into account because there are different opinions regarding the checks: for example, Yu *et al.* (2004) concluded that the pTRM-tail can only be detected reliably when the laboratory field is parallel to the NRM with the magnitude twice as large as the ancient field, whereas Biggin (2006) showed that reliable pTRM-tail checks can be performed if the laboratory field makes a large angle rela-

tive to the NRM. Nonetheless, the checks never show large pT$_M$RM-tails in any of the results. When analysing the results of the perpendicular method, an additional criterion of $89.9° < \theta_1 + \theta_2 < 90.1°$ for the selected linear segment was adopted, where θ_1 and θ_2 are angles between the observed remanence vector and the isolated NRM vector, and the observed remanence vector and the vector of the applied field direction, respectively.

Four specimens from the perpendicular method and eight specimens from the double heating experiment gave acceptable paleointensity results. They are summarized in Table 4. The resultant Arai plots give single slopes (Fig. 9(A) and (B)) except for one specimen (DX08-07-2c, Fig. 9(C) and (D)). If this two-sloped result is omitted (as was done for the Thelleir results), the paleointensities range between 7.8 μT and 28.6 μT with quality factors ranging from 3.59 to 34.1.

The perpendicular experiment success rate was extremely low (8%) when compared with the double heating experiment (36%). This is because (1) the present samples prepared for the microwave experiment often contained a certain amount of secondary remanences and (2) the double heating experiment was conducted after a series of perpendicular experiments (samples were more carefully selected for the double heating experiment based on these results). Examples of the unsuccessful results are illustrated in Fig. 9(E) and (F).
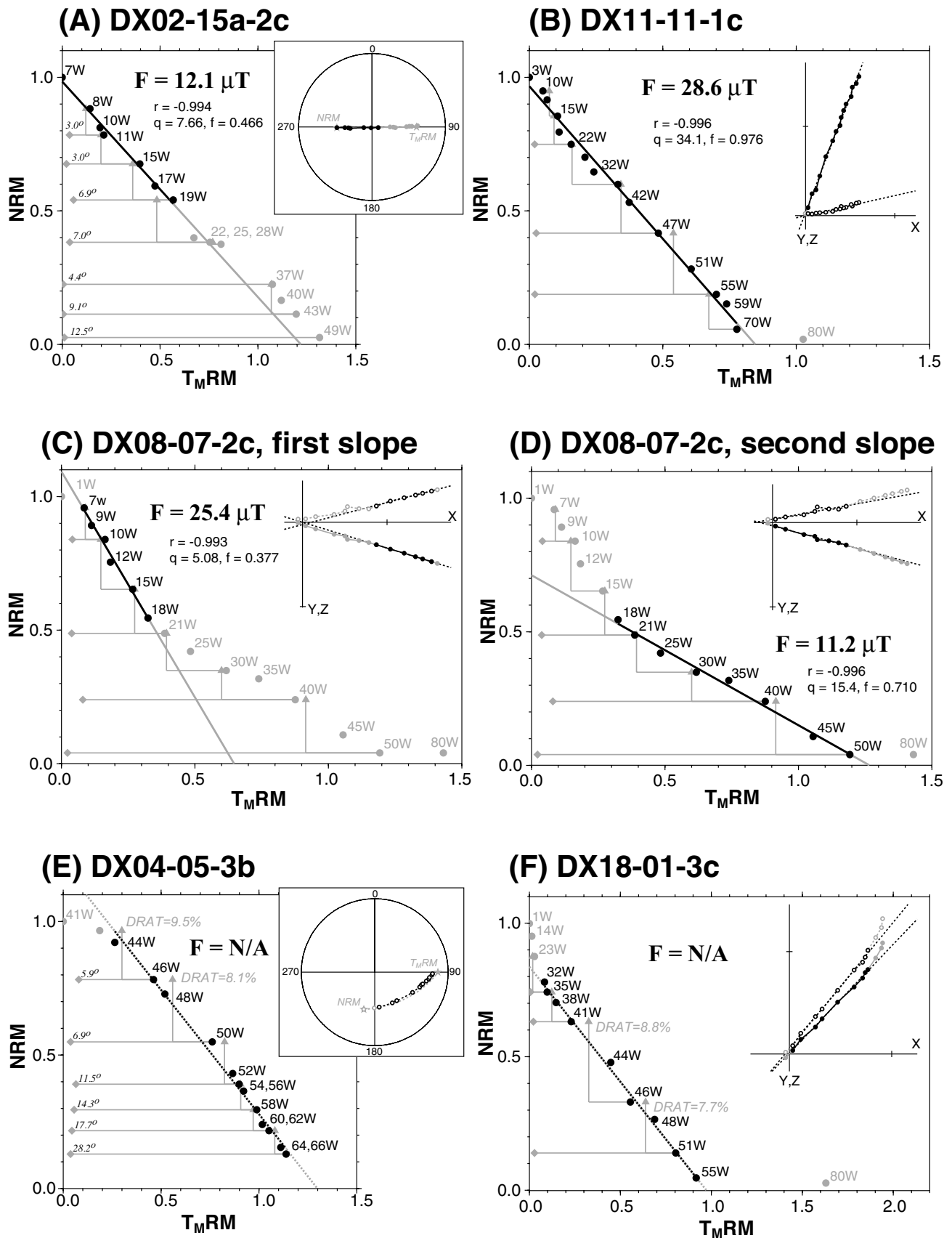
Fig. 9. Representative Arai plots from the results of the microwave Thellier experiment. (A) Example of the successful result using the perpendicular method. (B) Example of the successful result using the double heating method. (C and D) Examples of problematic two-sloped behavior observed in the double heating method. (E) Examples of the rejected result using the perpendicular method. (F) Example of rejected results using the double heating method. In (A) and (E), stereo plots with the isolated NRM direction (open stars) and the T_MRM direction (closed stars) are indicated. Note that angles between the isolated NRM direction and the directions of repeat zero-field steps are indicated in the upper-right of the pTRM-tail check results (closed diamonds) in (A) and (E).

5.4 Comparison of the results by the three methods

We have obtained paleointensity results by the three different methods. These results are compared in Fig. 7(A) for each site.

Four out of 13 successful Thellier results (except for the two-sloped results) came from cores yielding successful LTD-DHT Shaw results. Some pairs of samples give concordant answers whereas other pairs show inconsistent paleointensities (red circles in Fig. 7(B)). The *t*-test for paired samples on these data conclude that both data are statistically distingushable at the 80.0% confidence level. At the site-level, we can make a statistical comparison for three sites of DX06, 10 and 18, because they gave both Thellier and LTD-DHT Shaw paleointensities with the minimum number of three per site. All the site-mean Thellier paleointensities are higher than the LTD-DHT Shaw paleointensities (red circles in Fig. 7(C)), though the difference is only significant in the result from DX18 considering uncertainties of two standard deviations.

Eight microwave Thellier results can be compared with the LTD-DHT Shaw dataset (they were obtained from same cores). Paired results generally agree well (green squares in Fig. 7(B)), and the *t*-test for paired samples on these data show that both results are statistically indistingushable at the 95.2% confidence level. A statistical comparison at the site-level is only possible for DX02, and the site-mean microwave Thellier paleointensity appears to be higher than the site-mean LTD-DHT Shaw paleointensity (green squares in Fig. 7(C)). However, it is not statistically significant if we consider uncertainties of two standard deviations.

The comparisons show that the Thllier paleointensities tend to be higher than the LTD-DHT Shaw values, though the difference is sometimes not statistically significant. Similar observations are reported from three historical lava flows in Hawaii and Japan, the LTD-DHT Shaw method obtained correct paleointensities from these flows (Yamamoto *et al.*, 2003; Mochizuki *et al.*, 2004; Oishi *et al.*, 2005). In contrast, the comparisons seem to support similar quality of the LTD-DHT Shaw and the microwave Thellier results. Recent studies have revealed that the microwave Thellier method on volcanic rocks tends to give lower paleointensities than the conventional Thellier method (Bohnel *et al.*, 2003; Gratton *et al.*, 2005; Herrero-Bervera and Valet, 2005; Hill *et al.*, 2006). The same is true for the comparison between the LTD-DHT Shaw and the Thellier methods, as discussed in the above.

6. Discussion

6.1 Independency of the cooling units

We have obtained meaningful paleodirections from 21 sites (Section 4). As mentioned in Section 2, some of the sites possibly belong to the same cooling units and were tentatively classifeid as the same flow in Fig. 1. In order to evaluate such possibilities, we compared their paleodirections. By the proximity of sites, comparisons were made among following seven groups: (A) DX01, 02, 03, 04, 09 and 18, (B) DX05 and 17, (C) DX06, 07 and 08, (D) DX10 and 11, (E) DX13 and 14, (F) DX16 and 22, and (G) DX20 and 21 (Fig. 10). In the comparisons of the eastern sub-
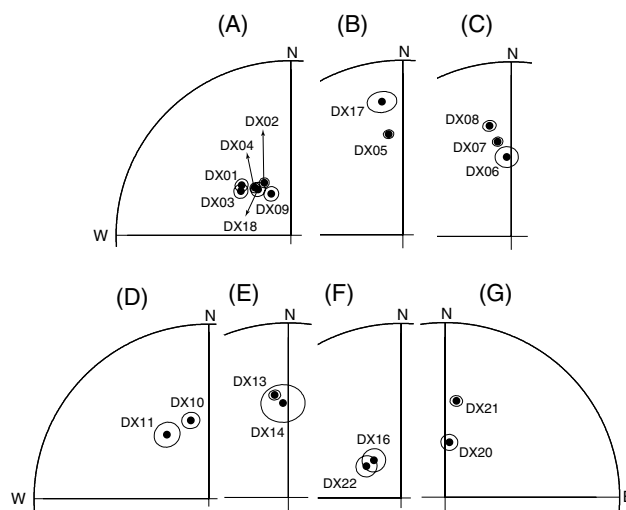
Fig. 10. Equal area projections of the paleodirections from possible same cooling units. (A) DX01, 02, 03, 04, 09 and 18, (B) DX05 and 17, (C) DX06, 07 and 08, (D) DX10 and 11, (E) DX13 and 14, (F) DX16 and 22, and (G) DX20 and 21. The solid circles with ovals around them are site-mean paleodirections and their 95% confidences.

group ((A)–(C)), three sites classified as sole units in Fig. 1 (DX06, 09 and 17) were taken into account because they probably originated from the nearest scoria cones.

In the comparison of (B), (C), (D) and (G), their paleodirections do not overlap by ovals of α_{95} (Fig. 10(B), (C), (D) and (G)). It is reasonable therefore to consider that these sites (DX05, 06, 07, 08, 10, 11, 17, 20 and 21) are independent. In contrast, the comparisons of (E) and (F) show overlapping α_{95} ovals (Fig. 10(E) and (F)). Applications of the statistical test of McFadden and Lowes (1981) does not distinguish between the two means at the 95% confidence level. We therefore treat the sites DX13 and DX14, and DX16 and DX22 as belonging to the same cooling units. These two units are referred to as DX13+14 and DX16+22.

The comparison of (A) is a little complicated since some α_{95} ovals overlap but others do not (Fig. 10(A)). Judging from the overlaps and the results of the statistical test by McFadden and Lowes (1981), the sites DX01 and DX03, DX04 and DX18, and DX02 and DX18 belong to the same cooling units. The test rejected a common mean of the sites DX02 and DX04. Because the site-mean LTD-DHT Shaw paleointensities are obtained as 6.80±1.52, 16.9±2.0 and 19.1±2.9 μT for the sites DX02, DX04 and DX18 (Table 1), it seems reasonable to treat sites DX04 and DX18 as coming from the same cooling unit. As a result, we recognize four cooling units (DX01+03, DX04+18, DX02 and DX09) in the comparison of (A).

In summary, the 21 sites are judged to originate from 17 independent cooling units (Table 1). The discussions that follow are based on the results from these cooling units.

6.2 Paleosecular variation

Although there is a series of normal faults in the area of the western subgroup (Fig. 1), they do not seem to affect the paleodirection results. This is because (1) the geological evidence suggests that the lava emplacement post-dates the faulting (grabens formed by the faults are buried with lavas, Section 2) and (2) the mean paleodirections of the western

(A)

N = 17
Lat = 76.5
Long = 7.9
A_95 = 7.7

(B)

N =17
I_m = 53.0
D_m = 345.1
α_95 = 6.9

GAD:
Inc = 59.3

(C)

Model G for IGRF1985
(McFadden et al.,1988; 1991)

Datong

Model G for the last 5 myr
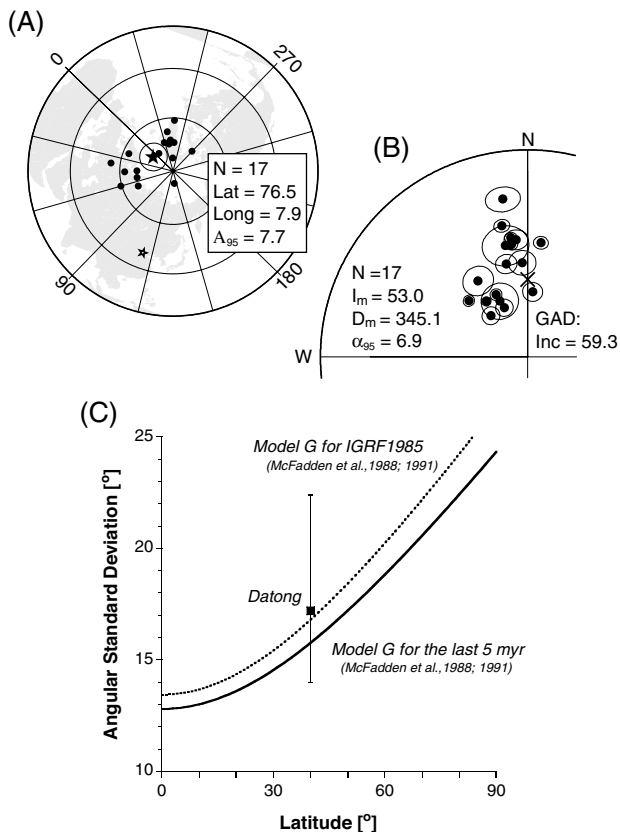*(McFadden et al.,1988; 1991)*

Fig. 11. (A) An equal area plot of 17 site-mean VGPs (solid circles). The solid star and an oval around it are the grand mean and its 95% confidence. The open star indicates the site location. (B) An equal area plot of 17 site-mean paleodirections (solid circles) with their associated 95% confidences (ovals around the circles). Direction of the geocentric axial dipole field (GAD) is also shown (cross). (C) Latitude dependence of the angular standard deviations (ASDs) of VGPs. Solid and dotted curves are the models by McFadden *et al.* (1988, 1991) for the IGRF1985 and the last 5 myr, respectively. The ASD calculated for the present dataset (Datong, N=17) is indicated by the solid square.

(Inc=55.9, Dec=347.3, A_95=11.4 and N=7) and eastern (Inc=51.0, Dec=343.8, A_95=9.8 and N=10) subgroups are indistinguishable.

The paleodirection results give a mean VGP position of (76.5°N, 7.9°E) with A_95=7.7 (N=17). This is statistically distinct from geographic north (Fig. 11(A)), indicating that the present dataset did not average out paleosecular variation. In fact, the dataset shows two clusters of paleodirections: one with a steep inclination and a westerly deflected direction and the other near the GAD (geocentric axial dipole field) direction (Fig. 11(B)). This suggests that the present samples might record the paleomagnetic field during two different short periods. These periods are possibly during 0.30 and 0.40 Ma because Hurford and Chen (1986) reported major volcanism in the Datong area during this period.

The present dataset yields an angular standard deviation (ASD) of 17.2° around the mean VGP position. It is consistent with the paleosecular variation model of McFadden *et al.* (1988, 1991) (Fig. 11(C)). However, we think this is fortuitous because there are two clusters of mean VGP positions (Fig. 11(A)) which are coming from the clustered paleodirections (Fig. 11(B)). The centers of the two clusters

(A)

LTD-DHT Shaw, Datong

Ave. = 3.79
σ = 1.94
N = 8

Ave.

(B)

T+ data

(1) 0-0.20 Ma
(2) 0.20-0.78 Ma

(1)+(2)

(2)

(1) + (2) Ave. = 7.49
σ = 3.06
N = 39

(2) Ave. = 5.91
σ = 1.74
N = 14
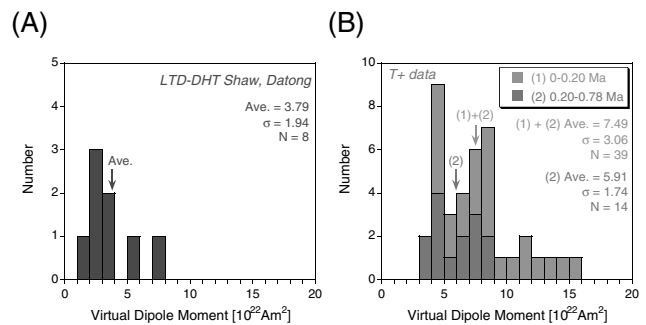
Fig. 12. (A) A histogram of VDMs for the selected LTD-DHT Shaw data presently obtained. An arrow indicates the average. (B) A same histogram shown for the selected Thellier data of (1) 0–0.20 Ma (light gray) and (2) 0.20–0.78 Ma (dark gray). Averages for datasets of (2) and (1) + (2) are indicated by arrows.

are distinct from each other, and the mean VGP is located between the two (Fig. 11(A)). This may result in the apparently reasonable ASD value. Thus, we think that the present dataset itself is not suitable to use for discussion of the paleosecular variation, although it can contribute to the time-averaged field global database as in similar way to Tauxe *et al.*'s (2004) study.

6.3 Average dipole moments during the middle to early Brunhes Chron

The LTD-DHT Shaw dataset presented here consists of 66 successful paleointensity results (Table 2). We know that the precision of the flow-mean LTD-DHT Shaw paleointensity is about 10% (standard deviation relative to the mean) based on results from historical lava flows (Yamamoto *et al.*, 2003; Mochizuki *et al.*, 2004; Oishi *et al.*, 2005). Flow-mean LTD-DHT Shaw paleointensities giving within-flow variabilities more than 10% might have to be discarded to avoid obtaining incorrect information. For paleointensities from older volcanic rocks, it may be reasonable to recognize within-flow variability of 20% as acceptable considering their age (e.g. they may have undergone a certain amount of weathering). From the dataset, eight acceptable site-mean LTD-DHT Shaw paleointensities can be selected by the following criteria.

(1) The minimum number of successful paleointensities per flow is three (N≥3).
(2) The maximum standard deviation of the flow-mean paleointensity is 20% (σ ≤ 20%).

They are from the six units of the eastern subgroup (DX04+18, DX02, DX07, DX08, DX09 and DX17) and the two units of the western subgroup (DX16+22 and DX11). These give virtual dipole moments (VDMs) of 1.13–7.34×10^22 A m^2 with an average and a standard deviation of 3.79×10^22 A m^2 and 1.94×10^22 A m^2, respectively (Fig. 12(A)).

To compare this average with the existing Thellier data, flow-mean paleointensity data by the Thellier method with pTRM checks (T+ data) are selected from the latest paleointensity database (PINT03; Perrin and Schnepp, 2004) by the same criteria. The selection was made on data spanning the Brunhes Chron (0–0.78 Ma). Because the selected data from the LTD-DHT Shaw dataset yield VGP latitudes
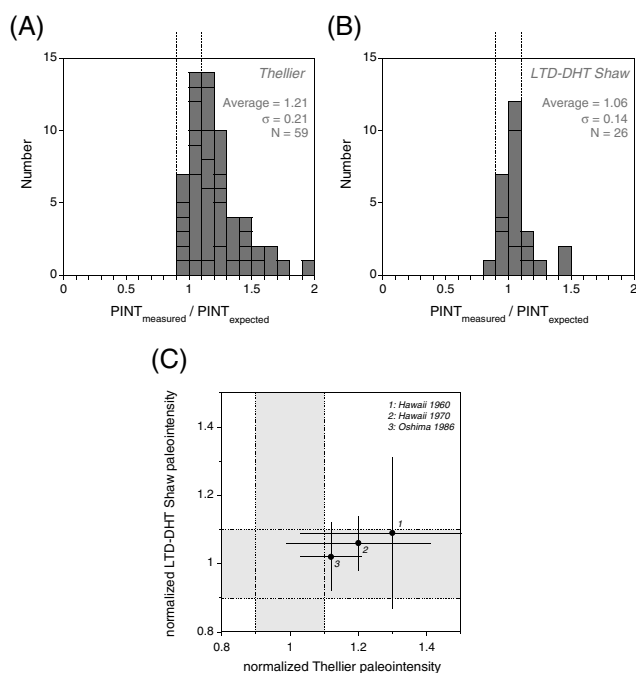
Fig. 13. (A) A histogram of Thellier paleointensity results obtained from historical basaltic lava flows (Tanaka and Kono, 1991; Tanaka *et al*., 1995a; Calvo *et al*., 2002; Yamamoto *et al*., 2003; Mochizuki *et al*., 2004; Oishi *et al*., 2005). Because strengths of the geomagnetic field are known at their eruption ages, results ($PINT_{measured}$) are normalized by the expected field intensities ($PINT_{expected}$). Dotted lines indicate ±10 percent limits of the expected values (0.9 and 1.1). (B) A same histogram for LTD-DHT Shaw paleointensity results obtained from historical basaltic lava flows (Yamamoto *et al*., 2003; Mochizuki *et al*., 2004; Oishi *et al*., 2005). (C) Comparisons of the flow-mean paleointensities obtained from the three historical flows (Hawaii 1960, 1970 and Oshima 1986). Horizontal and vertical axes indicate the normalized Thellier and LTD-DHT Shaw paleointensities by the expected field intensities (1.0 corresponds to the expected values). Error bars indicate one standard deviations.

of 59.4–74.6°N, the data are further screened by constraining VGP latitudes to be between 60.0°N and 75.0°N. This criterion seems to enable a statistically valid comparison though the LTD-DHT Shaw dataset is not averaging out paleosecular variation (Section 6.2). Both the statistical model (Tauxe and Kent, 2004) and the observational evidence (Tanaka *et al*., 1995b) suggest that VDMs are dependent on the associated VGP latitudes for the past few million years. 39 Thellier data remain and they give VDMs of $3.10–15.5 \times 10^{22}$ A m² with an average and standard deviation of 7.49×10^{22} A m² and 3.06×10^{22} A m², respectively (Fig. 12(B)). The Thellier average is almost twice as large as the LTD-DHT Shaw average. The *t*-test shows that both datasets are statistically distinguishable at the 99.8% confidence level. Although over a different time period, Yamamoto and Tsunakawa (2005) reached a similar conclusion from volcanic rocks spanning the last 5 m.y. from the Society Islands in French Polynesia. Using the LTD-DHT Shaw method, they obtained a mean VADM (virtual axial dipole moment) of 3.64×10^{22} A m² (standard deviation of 2.10×10^{22} A m²), which is almost half of the average of selected contemporaneous Thellier data (7.46×10^{22} A m², N=458).

Tauxe and Love (2003) reported that average VADMs are different between early Brunhes (0.40–0.78 Ma, 6.52×10^{22} A m²) and late Brunhes (0–0.40 Ma, 8.02×10^{22} A m²) based on analyses of cumulative distribution functions for the Thellier paleointensity database constructed by Juarez and Tauxe (2000). Because the geochronology studies on the Datong volcanic rocks (Kaneoka *et al*., 1983; Hurford and Chen, 1986; Chen *et al*., 1992; Cheng *et al*., 2006) suggest volcanic activity prior to ~0.20 Ma (Section 2), the difference between the Thellier and the LTD-DHT Shaw averages (the former is 98% higher than the latter) might be an overestimate. We further screened the Thellier data by rejecting the data younger than 0.20 m.y.. The remaining 14 data results in an average VDM of 5.91×10^{22} A m² with a standard deviation of 1.74×10^{22} A m² (Fig. 12(B)). The difference between the Thellier and the LTD-DHT Shaw averages becomes small (the former is 56% higher than the latter) but still exists. The *t*-test shows that both datasets are statistically distinguishable at the 98.4% confidence level.

Recent studies have revealed that the Thellier method applied to historical volcanic rocks tends to overestimate paleointensities by as much as twice the expected values. Figure 13(A) is a histogram showing reported Thellier paleointensities from historical basaltic lava flows: Hawaii 1960 (Tanaka and Kono, 1991; Yamamoto *et al*., 2003), Hawaii 1970 (Oishi *et al*., 2005), Oshima 1951 (Tanaka *et al*., 1995a), Oshima 1986 (Tanaka *et al*., 1995a; Mochizuki *et al*., 2004) and Mt Etna 1928 (Calvo *et al*., 2002). It suggests that the Thellier paleointensities are systematically higher than the expected values, with an average overestimation of 21%. In contrast, the LTD-DHT Shaw method on the same historical flows (Hawaii 1960, Yamamoto *et al*., 2003; Hawaii 1970, Oishi *et al*., 2005; Oshima 1986, Mochizuki *et al*., 2004) give paleointensities in agreement with the expected values (Fig. 13(B)). Three historical lava flows were investigated by the both methods (Fig. 13(C)). The *t*-test concludes that the datasets shown in Fig. 13(A) and (B) are statistically distinguishable at the 99.96% confidence level.

As introduced in Section 5.2, there are four possible reasons for the high Thellier paleointensities: (1) MD grains, (2) cumulative laboratory alteration, (3) TCRM acquisition during natural cooling, and (4) differences in cooling-rate between natural and laboratory conditions. Many researchers seem to prefer reason (1) (e.g. Biggin, 2006) but it is still controversial. More rock magnetic and paleointensity investigations from historical lava flows are needed. The high Thellier paleointensities might be one possible reason for the difference between the Thellier and the LTD-DHT Shaw averages presently observed, though the amount of the difference (56%) is much higher than the rate of the overestimation (21%).

7. Conclusions

We have conducted rock magnetic and paleomagnetic measurements on Datong volcanic rocks from China formed during the mid to early Brunhes Chron.

(1) Several rock magnetic experiments suggest that the main remanence carriers in the present samples are

titanomagnetites with varying Ti content ($\sim$ TM0–TM60). They are considered to be mixtures of SD (and/or PSD) and MD particles.

(2) Meaningful site-mean paleodirections are obtained from 21 sites. Considering their α_{95} ovals, they are judged to originate from 17 independent cooling units.

(3) The 17 independent paleodirection data give a mean VGP position of (76.5°N, 7.9°E) with A_{95}=7.7 (N=17). This is statistically distinct from geographic north, indicating that the data do not average out paleosecular variation. Because the data show two paleodirectional clusters, samples might record the paleomagnetic field during two different short periods.

(4) These data yield an ASD of 17.2° around the mean VGP position and are consistent with the paleosecular variation model of McFadden *et al.* (1988, 1991). We think this is fortuitous as there are two clusters of mean VGP positions and the mean VGP is located between the two; this may result in the apparently reasonable ASD value.

(5) Paleointensity measurements have been made using three different methods. The DHT and LTD-DHT Shaw methods, the Thellier method, and the microwave Thellier method applied to 119, 29 and 73 specimens give 66, 16 and 12 successful results, respectively (success rates are 55, 55 and 16%). We categorize the DHT and the LTD-DHT Shaw methods as a one method because they are very similar except for some points. In fact, there is no systematic difference between the results from the DHT and LTD-DHT Shaw methods. We treat both results as the same dataset (LTD-DHT Shaw dataset).

(6) Some of the Thellier results agree well the LTD-DHT Shaw dataset whereas others give higher paleointensities. The microwave Thellier results generally agree with the LTD-DHT Shaw dataset.

(7) From the LTD-DHT Shaw dataset, eight acceptable site-mean LTD-DHT Shaw paleointensities are obtained. They give an average VDM of 3.79×10^{22} A m^2 with a standard deviation of 1.94×10^{22} A m^2 for the mid to early Brunhes Chron. This is 56% lower than the average VDM of 5.91×10^{22} A m^2 (standard deviation of 1.74×10^{22} A m^2) which is calculated from the selected Thellier data from the latest paleointensity database (PINT03; Perrin and Schnepp, 2004) using the same selection criteria. One possible reason for this difference might be systematic overestimations of paleointensities by the Thellier method on volcanic rocks.

References

Biggin, A. J., First-order symmetry of weak-field partial thermoremanence in multi-domain (MD) ferromagnetic grains: 2. Implications for Thellier-type palaeointensity determination, *Earth Planet. Sci. Lett.*, **245**, 454–470, 2006.

Biggin, A. J. and N. D. Thomas, The application of acceptance criteria to results of Thellier palaeointensity experiments performed on samples with pseudo-single-domain-like characteristics, *Phys. Earth Planet. Inter.*, **138**, 279–287, 2003.

Bohnel, H., A. J. Biggin, D. Walton, J. Shaw, and J. A. Share, Microwave palaeointensities from a recent Mexican lava flow, baked sediments and reheated pottery, *Earth Planet. Sci. Lett.*, **214**, 221–236, 2003.

Bowles, J., J. S. Gee, D. V. Kent, E. Bergmanis, and J. Sinton, Cooling rate effects on paleointensity estimates in submarine basaltic glass and implications for dating young flows, *Geochem. Geophys. Geosyst.*, **6**, Q07002, doi:10.1029/2004GC000900, 2005.

Bureau of Geology and Mineral Resources of Shanxi Province, Regional geology of Shanxi Province, *Beijing: Geological Publishing House, 780 pp (in Chinese)*, 1989.

Calvo, M., M. Prevot, M. Perrin, and J. Riisager, Investigating the reasons for the failure of paleointensity experiments: a study on historic lava flows from Mt. Etna (Italy), *Geophys. J. Int.*, **149**, 44–63, 2002.

Chauvin, A., P. Roperch, and S. Levi, Reliability of geomagnetic paleointensity data: the effects of the NRM fraction and concave-up behavior on paleointensity determinations by the Thellier method, *Phys. Earth Planet. Inter.*, **150**, 265–286, 2005.

Chen, W. J., D. M. Li, T. M. Dai, Z. P. PU, R. X. Liu, Q. LI, J. Z. Shun, X. Wang, E. Jager, A. J. Hurford, and H. R. Pfeifer, The K-Ar age and excess Ar of Quaternary basalt in Datong, In *The Age and Geochemistry of Cenozoic Volcanic Rock in China (ed. R. X. Liu)*, pp. 81–92, Beijing: Seismological Press (in Chinese), 1992.

Cheng, S. P. and G. Z. Yang, Segmented variations in tectonic geomorphology of Datong-Yangyuan fault zone, NW Beijing, China, *J. Balkan Geophs. Soc.*, **2**, 46–62, 1999.

Cheng, S. P., C. Y. Li, G. Z. Yang, and S. W. Zhou, Differentiating Pleistocene tectonically driven and climate-related fluvial incision: the Sanggan River, Datong Basin, North China, *Geol. Mag.*, **143**, 393–410, 2006.

Coe, R. S., S. Gromme, and E. A. Mankinen, Geomagnetic paleointensities from radiocarbon-dated lava flows on Hawaii and the question of the pacific nondipole low, *J. geophys. Res.*, **83**, 1740–1756, 1978.

Coe, R. S., S. Gromme, and E. A. Mankinen, Geomagnetic paleointensities from excursion sequences in lavas on Oahu, Hawaii, *J. geophys. Res.*, **89**, 1059–1069, 1984.

Day, R., M. Fuller, and V. A. Schmidt, Hysteresis properties of titanomagnetites: grain-size and compositional dependence, *Phys. Earth Planet. Inter.*, **13**, 260–267, 1977.

Deng, Q. D., N. Yonekura, X. W. Xu, Y. Suzuke, C. Y. Wang, T. Akira, Z. Z. Su, and Y. P. Wang, Study on the late Quaternary Kinematics of the northern piedmont fault of the Liuleng Mountain, *Seismology and Geology*, **16**, 339–343 (in Chinese), 1994.

Duan, R. T. and Z. J. Fang, Neotectonic characteristics of the northern piedmont fault of the Liuleng Mountain, *Seismology and Geology*, **17**, 205–213 (in Chinese), 1995.

Dunlop, D. J., Theory and application of the Day plot (Mrs/Ms versus Hcr/Hc) 1. Theoretical curves and tests using titanomagnetite data, *J. Geophys. Res.*, **107**, 3, 10.1029/2001JB000486, 2002.

Fox, J. M. W. and M. J. Aitken, Cooling rate dependence of the thermoremanent magnetization, *Nature*, **283**, 462–463, 1980.

Goguitchaichvili, A., J. Urrutia-Fucugauch, L. M. Alva-Valdivia, J. Morales, J. Riisager, and P. Riisager, Long-term variation of geomagnetic field strength: a cautionary note, *Eos Trans. AGU*, **85**, 209–212, 2004.

Gratton, M. N., J. Shaw, and E. Herrero-Bervera, An absolute palaeointensity record from SOH1 lava core, Hawaii using the microwave technique, *Phys. Earth Planet. Inter.*, **148**, 193–214, 2005.

Heider, F., D. J. Dunlop, and H. C. Soffel, Low-temperature and alternating field demagnetization of saturation remanence and thermoremanence in magnetite grains (0.037μm to 5mm), *J. Geophys. Res.*, **97**, 9371–9381, 1992.

Herrero-Bervera, E. and J. P. Valet, Absolute paleointensity and reversal records from the Waianae sequence (Oahu, Hawaii, USA), *Earth Planet. Sci. Lett.*, **234**, 279–296, 2005.

Hill, M. J. and J. Shaw, Paleointensity results for historic lavas from Mt Etna using microwave demagnetization/remagnetization in a modified Thellier-type experiment, *Geophys. J. Int.*, **139**, 583–590, 1999.

Hill, M. J. and J. Shaw, Magnetic field intensity study of the 1960 Kilauea lava flow, Hawaii, using the microwave paleointensity technique, *Geophys. J. Int.*, **142**, 487–504, 2000.

Hill, M. J., J. Shaw, and E. Herrero-Bervera, Palaeointensity record through the Lower Mammoth reversal from the Waianae volcano, Hawaii, *Earth Planet. Sci. Lett.*, **230**, 255–272, 2005.

Hill, M. J., J. Shaw, and E. Herrero-Bervera, Determining palaeointensity from the Gilbert Gauss Reversal recorded in the Pufu Heleakala lava section, Waifanae Volcano, Oahu, Hawaii, *Earth Planet. Sci. Lett.*, **245**, 29–38, 2006.

Hurford, A. J. and W. J. Chen, Dating the Datong volcanics in North China: the new K-Ar-Standard, *Schweiz. Mineral. Petrogr. Mitt.*, **66**, 483, 1986.

International Association of Geomagnetism and Aeronomy (IAGA), Division V, Working Group VMOD: Geomagnetic Field Modeling, The 10th-Generation International Geomagnetic Reference Field, *Geophys. J. Int.*, **161**, 561–565, 2005.

Juarez, M. T. and L. Tauxe, The intensity of the time-averaged geomagnetic field: the last 5 Myr, *Earth Planet. Sci. Let.*, **175**, 169–180, 2000.

Kaneoka, I., K. Notsu, and C. Liu, K-Ar age and Sr isotopic ratio of a Pleistocene Datong basalt, China, *Bull. Volcano. soc. Japan*, **28**, 75–78, 1983.

Kirschvink, J. L., The least-squares line and plane and the analysis of paleomagnetic data, *Geophys. J. R. Astr. Soc.*, **62**, 699–718, 1980.

Kissel, C. and C. Laj, Improvements in procedure and paleointensity selection criteria (PICRIT-03) for Thellier and Thellier determinations: application to Hawaiian basaltic long cores, *Phys. Earth Planet. Inter.*, **147**, 155–169, 2004.

Kono, M. and N. Ueno, Paleointensity determination by a modified thellier method, *Phys. Earth Planet. Inter.*, **13**, 305–314, 1977.

Kono, M., Y. Hamano, T. Nishitani, and T. Tosha, A new spinner magnetometer: principles and techniques, *Geophys. J. R. Astr. Soc.*, **67**, 217–227, 1984.

Kono, M., H. Kitagawa, and H. Tanaka, Use of automatic spinner magnetometer—AF demagnetizer system for magnetostratigraphy and paleosecular variation studies (abstract), in *Proc. 8th Scientific Assembly IAGA, 1997 Abstract book*, pp. 66, Uppsala, 1997.

Levi, S., The effect of magnetite particle size on paleointensity determinations of the geomagnetic field, *Phys. Earth Planet. Inter.*, **13**, 245–259, 1977.

Liu, J., J. Han, and Z. Guo, The Cenozoic volcanoes in Northeast China, *J. Geocsci. Res. NE Asia*, **5**, 7–15, 2002.

McFadden, P. L. and F. J. Lowes, The discrimination of mean directions drawn from Fisher distributions, *Geophys. J. R. Astr. Soc.*, **67**, 19–33, 1981.

McFadden, P. L. and M. W. McElhinny, The combined analysis of remagnetization circles and direct observations in paleomagnetism, *Earth planet. Sci. Lett.*, **87**, 161–172, 1988.

McFadden, P. L., R. T. Merrill, and M. W. McElhinny, Dipole/quadrupole family modeling of paleosecular variation, *J. Geophys. Res.*, **93**, 11583–11588, 1988.

McFadden P. L., R. T. Merrill, M. W. McElhinny, and S. Lee, Reversals of the Earth's magnetic field and temporal variations of the dynamo families, *J. Geophys. Res.*, **96**, 3923–3933, 1991.

Mochizuki, N., H. Tsunakawa, Y. Oishi, S. Wakai, K. Wakabayashi, and Y. Yamamoto, Palaeointensity study of the Oshima 1986 lava in Japan: implications for the reliability of the Thellier and LTD-DHT Shaw methods, *Phys. Earth Planet. Inter.*, **146**, 395–416, 2004.

Mochizuki, N., H. Tsunakawa, H. Shibuya, J. Cassidy, and I. E. M. Smith, Palaeointensities of the Auckland geomagnetic excursions by the LTD-DHT Shaw method, *Phys. Earth Planet. Inter.*, **154**, 168–179, 2006.

Morales, J., L. M. Alva-Valdivia, A. Goguitchaichvili, and J. Urrutia-Fucugauchi, Cooling rate corrected paleointensities from the Xitle lava flow: Evaluation of within-site scatter for single spot-reading cooling units, *Earth Planets Space*, **58**, 1341–1347, 2006.

Nagata, T., Y. Arai, and K. Momose, Secular variation of the geomagnetic total force during the last 5000 years, *J. Geophys. Res.*, **68**, 5277–5281, 1963.

Oishi, Y., H. Tsunakawa, N. Mochizuki, Y. Yamamoto, K. Wakabayashi, and H. Shibuya, Validity of the LTD-DHT Shaw and Thellier palaeointensity methods: a case study of the Kilauea 1970 lava, *Phys. Earth Planet. Inter.*, **149**, 243–257, 2005.

Ozima, M., M. Ozima, and S. Akimoto, Low temperature characteristics of remanent magnetization of magnetite—Self-reversal and recovery phenomena of remanent magnetization—, *J. Geomag. Geoelectr.*, **16**, 165–177, 1964.

Perrin, M. and E. Schnepp, IAGA paleointensity database: distribution and quality of the data set, *Phys. Earth Planet. Inter.*, **147**, 255–267, 2004.

Riisager, P. and J. Riisager, Detecting multidomain magnetic grains in Thellier paleointensity experiments, *Phys. Earth Planet. Int.*, **125**, 111–117, 2001.

Roberts, A. P., C. R. Pike, and K. L. Verosub, First-order reversal curve diagrams: A new tool for characterizing the magnetic properties of natural samples, *J. Geophys. Res.*, **105**, 28461–28475, 2000.

Rolph, T. C. and J. Shaw, A new method of paleofield magnitude correction for thermally altered samples and its application to Lower Carboniferous lavas, *Geophys. J. R. Astr. Soc.*, **80**, 773–781, 1985.

Selkin, P. A. and L. Tauxe, Long-term variations in palaeointensity, *Phil. Trans. Roy. Soc. Lond. A.*, **358**, 1065–1088, 2000.

Shaw, J., A new method of determining the magnitude of the paleomagnetic field. Application to five historic lavas and five archaeological samples, *Geophys. J. R. Astr. Soc.*, **76**, 637–651, 1974.

Shaw, J., D. Walton, S. Yang, T. C. Rolph, and J. A. Share, Microwave archaeointensities from Peruvian ceramics, *Geophys. J. Int.*, **124**, 241–244, 1996.

Shcherbakov, V. P. and V. V. Shcherbakova, On the suitability of the Thellier method of paleointensity determinations on pseudo-single-domain and multidomain grains, *Geophys. J. Int.*, **146**, 20–30, 2001.

Shcherbakova,V. V., V. P. Shcerbakov, and F. Heider, Properties of partial thermoremanent magnetization in pseudosingle domain and multidomain magnetite grains, *J. geophys. Res.*, **105**, 767–781, 2000.

Tanaka, H. and T. Kobayashi, Paleomagnetism of the late Quaternary Ontake Volcano, Japan: directions, intensities, and excursions, *Earth Planets Space*, **55**, 189–202, 2003.

Tanaka, H. and M. Kono, Preliminary Results and Reliability of Paleointensity Studies on Historical and ^{14}C Dated Hawaiian Lavas, *J. Geomag. Geoelectr.*, **43**, 375–388, 1991.

Tanaka, H., M. Kono, and S. Kaneko, Paleosecular variation of direction and intensity from two Pliocene-Pleistocene lava sections in southwestern Iceland, *J. Geomag. Geoelectr.*, **47**, 89–102, 1995a.

Tanaka, H., M. Kono, and H. Uchimura, Some global features of paleointensity in geological time, *Geophys. J. Int.*, **120**, 97–102, 1995b.

Tanaka, H., R. Kamizaki, and Y. Yamamoto, Palaeomagnetism of the Older Ontake Volcano, Japan: contributions to the palaeosecular variation for 750–400 Ka, the lower half of the Brunhes Chron, *Geophys. J. Int.*, **169**, 81–90, 2007.

Tauxe, L. and D. Kent, A Simplified Statistical Model for the Geomagnetic Field and the Detection of Shallow Bias in Paleomagnetic Inclinations: Was the Ancient Magnetic Field Dipolar?, Channell, J. E. T. *et al.*, eds., Geophysical Monograph, **145**, 101–116, 2004.

Tauxe, L. and J. J. Love, Paleointensity in Hawaiian Scientific Drilling Project Hole (HSDP2): Results from submarine basaltic glass, *Geochem., Geophys., Geosyst.*, **4**, 8702, doi:10.1029/2001GC000276, 2003.

Tauxe, L., C. Luskin, P. Selkin, P. Gans, and A. Calvert, Paleomagnetic results from the Snake River Plain: Contribution to the time-averaged field global database, *Geochem. Geophys. Geosyst.*, **5**, Q08H13, doi:10.1029/2003GC000661, 2004.

Thellier, E. and O. Thellier, Sur l'intensite du champ magnetique terrestre dans le passe historique et geologique, *Ann. Geophys.*, **15**, 285–376, 1959.

Thomas, N. D., M. J. Hill, and A. S. Garcia, Comparison of the Coe-Thellier-Thellier and microwave palaeointensity techniques using hightitanium titanomagnetites: results from a Tertiary basaltic intrusion from the Sydney Basin, New South Wales, *Earth Planet. Sci. Lett.*, **229**, 15–29, 2004.

Tsunakawa, H. and J. Shaw, The Shaw method of paleointensity determinations and its application to recent volcanic rocks, *Geophys. J. Int.*, **118**, 781–787, 1994.

Valet, J. P., Time variations in geomagnetic intensity, *Rev. Geophys.*, **41**, 1004, doi:10.1029/2001RG000104, 2003.

Xu, S. and D. J. Dunlop, Thellier paleointensity theory and experiments for multidomain grains, *J. Geophys. Res.*, **109**, B07103 doi:10.1029/2004JB003024, 2004.

Xu, X. W., N. Yonekura, S. Yasukiro, Q. D. Deng, Y. P. Wang, T. Akira, and C. Y. Wang, Geomorphic study on late quaternary irregular faulting along the northern piedmont of Liulengshan Range, Shanxi Province, China, *Seismology and Geology*, **18**, 169–181 (in Chinese), 1996.

Yamamoto, Y., Possible TCRM acquisition of the Kilauea 1960 lava, Hawaii: failure of Thellier paleointensity determination inferred from equilibrium temperature of the Fe-Ti oxide, *Earth Planets Space*, **58**, 1033–1044, 2006.

Yamamoto, Y. and H. Tsunakawa, Geomagnetic field intensity during the last 5 Myr: LTD-DHT Shaw palaeointensities from volcanic rocks of the Society lslands, French Polynesia, *Geophys. J. Int.*, **162**, 79–114, 2005.

Yamamoto, Y., H. Tsunakawa, and H. Shibuya, Palaeointensity study of the Hawaiian 1960 lava: implications for possible causes of erroneously high intensities, *Geophys. J. Int.*, **153**, 263–276, 2003.

Yu, Y., L. Tauxe, and A. Genevey, Toward an optimal geomagnetic field intensity determination technique, *Geochem. Geophys. Geosyst.*, **5**, Q02H07, doi:10.1029/2003GC000630, 2004.

Y. Yamamoto (e-mail: y.yamamoto@kochi-u.ac.jp), H. Tsunakawa, J. Shaw, and M. Kono